Renewable and Sustainable Energy Reviews 109 (2019) 606–618

Contents lists available at ScienceDirect

Renewable and Sustainable Energy Reviews

journal homepage: www.elsevier.com/locate/rser

Proton conducting oxides: A review of materials and applications for renewable energy conversion and storage

J. Kim[a,e,1], S. Sengodan[b,e,1], S. Kim[c,e], O. Kwon[e], Y. Bu[d,e], G. Kim[e,*]

[a] Department of Chemistry, University of Liverpool, Liverpool, L69 3BX, United Kingdom
[b] Department of Materials, Imperial College London, London, SW7 2BX, United Kingdom
[c] Materials Science and Engineering Program & Texas Materials Institute, University of Texas at Austin, Austin, Texas 78712, United States
[d] School of Environment Science and Engineering, Nanjing University of Information Science and Technology (NUIST), Nanjing, 210044, PR China
[e] School of Energy and Chemical Engineering, Ulsan National Institute of Science and Technology (UNIST), Ulsan, 44919, Republic of Korea

ARTICLE INFO

Keywords:
Proton conducting oxides
Protonic ceramic fuel cells
Solid oxide fuel cells
Hydrogen energy

ABSTRACT

Recent developments in proton conducting oxides (PCOs) present a promise of economic and sustainable energy conversion and storage devices such as protonic ceramic fuel cells, protonic ceramic electrolysis cells, gas purification, syn-gas membrane, and ammonia synthesis. This review provides a comprehensive overview of the development and recent trends in electrochemical cells based on the PCOs. Various protonic electrochemical cells are described here with basic working principles and critical parameters affecting the performance. Also, the electrochemical properties and recent progress on the PCO materials are reviewed and discussed. The overview of PCOs provides guidelines for the scientific-based rational design of PCO materials for the efficient protonic energy conversion and storage applications in academic and industrial fields.

1. Introduction

With the exponential growth in energy consumption and finite fossil fuel resources, the necessity for sustainable energy conversion and storage (ECS) devices are increasing [1]. Ceramic fuel cells have attracted attention because of their high energy conversion efficiencies and their potential applications in ceramic electrolysis cells, hydrogen pump, membrane reactors, ammonia synthesis, fuel reformers, and hydrogen sensors [2]. However, the intermediate to high operating temperature ($> 650\,^{\circ}C$) of conventional O^{2-} conducting ceramic fuel cells (*i.e.*, solid oxide fuel cells, SOFCs) is an obstacle to their commercialization, mainly because of significant degradation, sealing problems, and high thermal stress [3].

In this regard, extensive efforts have been devoted to lowering the operating temperature of ceramic fuel cells. After the first report of proton conductivity in oxide materials by Iwahara and co-workers in the 1980s, [4,5] protonic ceramic fuel cells (PCFCs) using proton conducting oxides (PCOs) have been considered as promising candidates for low temperature operation ($< 650\,^{\circ}C$) because of their high ionic conductivity and low activation energy for H^{+} transport [6]. The low operating temperature of PCFCs provides great benefits such as reduction of plant costs, and wider material choices for system components [7]. Moreover, since both component inter-diffusion and radiative heat transfer exponentially drop off below 600 °C, the primary performance degradation mechanism can be eliminated [8].

After decades of development on the proton-conducting electrolyte materials, their fundamental properties have been reviewed [9,10] and excellent electrode materials have been developed [11,12] to further improve electrochemical performance. These advances of materials and technologies opened the possibility of significant improvement for the performance of various applications based on the PCOs such as protonic ceramic fuel cells, protonic ceramic electrolysis cells, gas purification, syn-gas membrane, and ammonia synthesis [13,14]. The purpose of this paper is to provide an understanding and ideas on developing new materials using protonic properties, and to provide guidelines on the material choices and possible applications in academic and industry fields. This review paper starts with the overview of possible ceramic electrochemical applications based on the proton conducting oxides with their backgrounds and brief theoretical principles of critical parameters affecting the performance. After the discussion of potential applications, numerous researches on the materials for these applications have been comprehensively reviewed in each section. The overview of proton conducting oxide materials provides the most recent progress obtained by various approaches to develop materials. This

* Corresponding author.
E-mail address: gtkim@unist.ac.kr (G. Kim).
[1] These authors contributed equally to this work.

https://doi.org/10.1016/j.rser.2019.04.042
Received 20 January 2019; Received in revised form 28 March 2019; Accepted 12 April 2019
Available online 24 April 2019
1364-0321/

review concludes with presenting the challenges and future directions.

2. Applications

Research using proton conducting oxides made a beginning in the 1990s, and several proton-conducting oxides have been explored for various kinds of applications. In this section, protonic applications are classified with (1) energy storage and conversion and (2) chemical synthesis. In energy storage and conversion application proton conducting oxides, the electromotive force (EMF) is utilized to drive the protons between the electrodes; while in chemical synthesis, EMF, catalysis, and preferential protonic transport are utilized.

2.1. Energy conversion and storage

2.1.1. Protonic ceramic fuel cells

Among hydrogen energy systems, SOFCs have received tremendous attention as promising energy conversion devices for high efficiency and low emission renewable energy [15,16]. Nevertheless, the required high operating temperatures of 800–1000 °C lead to critical problems including: [17]

1. Material limitations (corrosion, chemical inter-diffusion, and reactions between components)
2. Operating complexities
3. Expensive systems costs
4. Rapid performance degradation
5. Slow start-up and shutdown cycles
6. Limiting applicability in the portable power and transportation markets

To resolve these problems, low-temperature SOFCs (LT-SOFCs) with an operating temperature under 650 °C have been suggested as a solution [8,18]. The low operating temperature reduces system cost due to the wider range of material choices for the interconnector and compressive non-glass/ceramic seals [19,20]. Even with the benefits, poor activity and a corresponding low power density are significant barriers to low temperature operation [21,22].

In this regard, PCFCs have been proposed as promising LT-SOFCs due to their low activation energy (0.4–0.6 eV) for proton transport, which is approximately half of the typical oxygen ion transport activation energy [23,24]. Based on the proton conduction at the electrolyte, the following equations (Equations (1)–(3)) are proposed for the PCFC:

$$2H_2 \rightarrow 4H^+ + 4e^- \text{ (Hydrogen electrode, anode)} \quad (1)$$

$$4H^+ + O_2 + 4e^- \rightarrow 2H_2O \text{ (Air electrode, cathode)} \quad (2)$$

$$2H_2 + O_2 \rightarrow 2H_2O \text{ (Overall reaction)} \quad (3)$$

The hydrogen supplied to the anode is catalytically dissociated into protons and electrons and released through the electrolyte and the leading wire, respectively [25,26]. As shown in Fig. 1a, the proton transported through the electrolyte reacts with oxygen to produce water at the cathode. In contrast to a typical SOFC where water is generated at the anode, water production at the cathode of the PCFC improves fuel utilization and efficiency by suppressing fuel dilution [27,28].

However, their practical use is yet to be realized by several barriers such as:

1. Poor sinterability
2. Blocking nature of grain boundary
3. Low chemical stability of proton conducting oxides.
4. Large electrode overpotentials of cathodes.

In an effort to solve these problems, many researchers have tried to develop new electrolyte and cathode materials or multi-layered anode support structure and have significantly improved the power density of PCFCs. The highest PCFC power density is reported by Haile et al. using a $PrBa_{0.5}Sr_{0.5}Co_{1.5}Fe_{0.5}O_{5+\delta}$ (PBSCF) cathode and $BaZr_{0.4}Ce_{0.4}Y_{0.1}Yb_{0.1}O_{3-\delta}$ (BZCYYb) electrolyte. They achieved exceptionally high power density (1.1 W cm^{-2} at 650 °C) and stability (700 h at 550 °C) [25]. More fundamental studies and history on the material development are described in the later sections in three parts: cathode, electrolyte, and anode.

2.1.2. Protonic ceramic electrolysis cells

Among the clean and renewable energy sources, hydrogen energy is considered as a next-generation energy technology to replace fossil energy [4]. However, conventional hydrogen production using a steam reforming process with fossil resources promotes fossil fuel depletion and CO_2 emissions. In this regard, steam electrolysis has received tremendous attention due to the increased demand for H_2 production technology with low environmental impact and high efficiency [30,31]. For the water-splitting reaction, thermodynamic data for steam electrolysis is shown in Fig. 2 at a steam pressure of 1 atm based on Equation (4), where ΔH is total energy demand, ΔG is the electrical energy demand, and $T\Delta S$ is the heat energy demand.

$$\Delta H = \Delta G + T\Delta S \quad (4)$$

Due to the water phase transition (liquid to gas), the total energy demand (ΔH) significantly drops off at 100 °C. As temperature increases, the thermal energy ($T\Delta S$) is increased and thereby the electrical energy demand (ΔG) reduced implying that the high-temperature SOECs are more effective (low cost, less electricity) than low-temperature water electrolysis systems if the heat energy demand can be compensated by external sources like waste heat from industries [32,33].

With proton-conducting oxides, the principle of the steam electrolysis can be expressed by the following equations, (Equations (5) and (6)):

$$H_2O \rightarrow 2H^+ + 2e^- + 1/2O_2 \text{ (Air electrode, anode)} \quad (5)$$

$$2H^+ + 2e^- \rightarrow H_2 \text{ (Hydrogen electrode, cathode)} \quad (6)$$

As shown in the schematic illustration of steam electrolysis using a proton-conducting electrolyte (Fig. 1b), steam is dissociated into oxygen and protons at the air electrode with a current supply, while pure and dry hydrogen is evolved at the hydrogen electrode.

Kim et al. suggested a hybrid-SOEC system based on both oxygen ion and proton conducting properties of the BZCYYb electrolyte [34]. By providing steam to both electrodes, the hybrid-SOEC system (see Fig. 3) allows simultaneous oxygen-SOEC and proton-SOEC operation. Compared to conventional oxygen-SOEC and proton-SOEC, the hybrid-SOEC shows a higher current density of 3.16 A cm^{-2} at 1.3 V and 750 °C with a stable operation for 60 h.

2.2. Chemical production

2.2.1. Purification

In a hydrogen separation membrane based on dense proton conductors, a hydrogen chemical potential gradient will be applied to drive the flow of hydrogen through the ceramic membrane. The chemical potential gradient across a proton conducting ceramic membrane will be controlled by the concentration gradient, temperature, and electric field. Fig. 4a illustrates the design of a ceramic proton conducting membrane with electronic-protonic conductivity. When the chemical potential of hydrogen across the membrane is unequal, then:

$$\mu(H_2)^{(2)} < \mu(H_2)^{(1)} \quad (7)$$

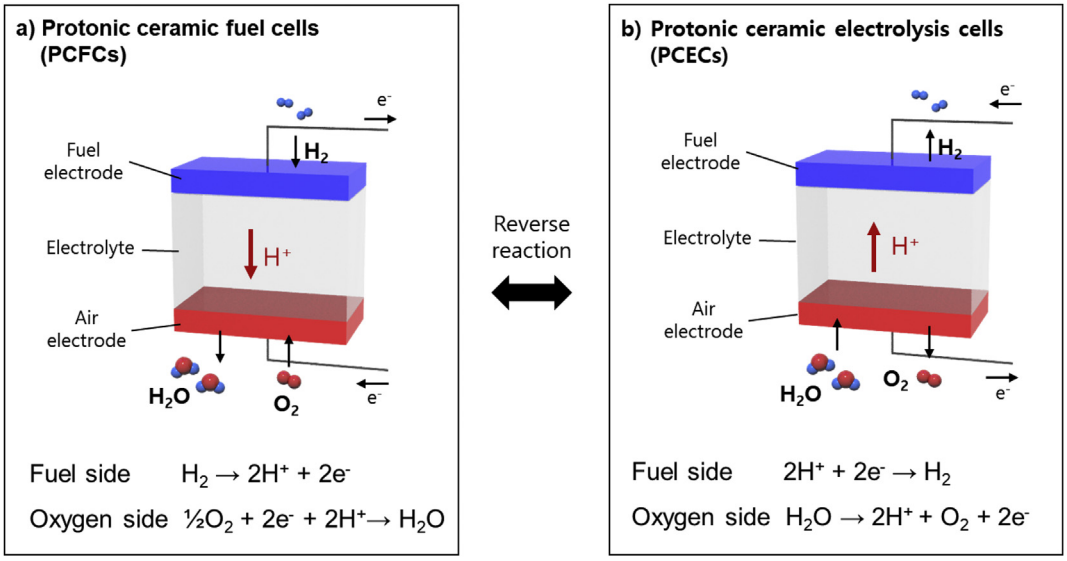

Fig. 1. Schematic illustration of the working principle for PCFCs and PCECs.

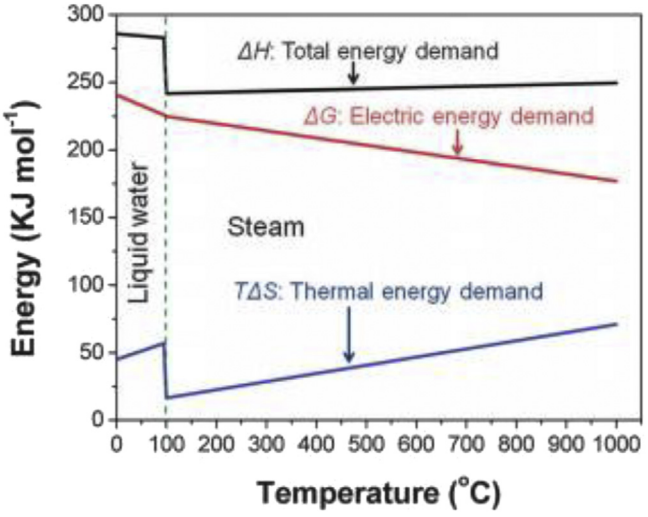

Fig. 2. Electric, thermal, and total energy demand for H_2O electrolysis as a function of temperature, showing the electric energy demand decreasing considerably which is compensated by the thermal energy demand increasing with increasing operating temperatures, reproduced with permission [29].

which is equivalent to partial pressure of H_2 across the membrane:

$$p(H_2)^{(2)} < p(H_2)^{(1)} \quad (8)$$

Then the diffusion of electrons and protonic defects takes place through the proton conducting oxide membrane to the low partial pressure side of the dense ceramic membrane. The hydrogen separation process through the ceramic proton conductor involves several steps:

1. Diffusion and dissociative adsorption of hydrogen molecules on the feed side.
2. Ambipolar diffusion of protonic defects in the ceramic proton conducting phase and electrons in the electronic phase of the membrane.
3. Proton reduction at the sweep side of the membrane.
4. Hydrogen re-association and desorption of hydrogen to move away from the surface.

Depending on the membrane materials, the rate of hydrogen oxidation and/or electron conductivity determine the hydrogen permeation rate of the proton conducting membrane and achieving high hydrogen flux remains the greatest difficulty for the development of proton conducting separation membranes. It was estimated that both protonic conductivity and electronic conductivity should be higher than 0.1 S cm^{-1}, which are required for the separation membrane to be useful for hydrogen separation [35]. Among the proton conducting perovskite-type oxides, $SrCeO_3$, $BaCeO_3$, and $BaZrO_3$ have been studied extensively. Different trivalent cations such as Y, Yb, Sm, Nd, Eu, Sc, and Tb and transition metal dopants (Fe and Mn) have been used to partially substitute at Ce/Zr sites. Despite the intensive efforts to enhance the hydrogen flux in single-phase proton conducting membranes, the hydrogen permeation flux is still low due to poor electronic conductivity. To further improve hydrogen flux, dual phase ceramic membranes were developed in which the composite of the electron conducting phase and the proton conducting oxide phase. Among the dual phase membranes, Ni is used as the electron conducting phase because of its high conductivity, catalytic activity for hydrogen oxidization, mechanical stability, and low cost for membrane fabrication. Table 1 summarizes representative single-phase and dual-phase ceramic proton conducting membranes for hydrogen separation.

2.2.2. *Membrane reactors*

Syngas is a mixture of carbon monoxide and hydrogen and is a key intermediate in the chemical industry; it is primarily used in ammonia and methanol synthesis. Both syngas and hydrogen can be synthesized by the reforming (steam reforming, partial oxidation reforming, and auto-thermal reforming) of methane or other fuels such as coal. Due to energy savings and process intensification in the last few years, methane reforming at low temperature (400–600 °C) has been proposed to decrease the cost of the reforming process. The water gas shift reaction (WGS) and the methane steam reforming (MSR) convert CO and CH_4, respectively, into the mixture of CO_2 and H_2 by the following reaction:

$$H_2O + CO \rightleftarrows H_2 + CO_2 \ (\Delta H_{298} = -41 \text{ kJ mol}^{-1}) \quad (9)$$

$$CH_4 + 2H_2O \rightleftarrows 4H_2 + CO_2 \ (\Delta H_{298} = +165 \text{ kJ mol}^{-1}) \quad (10)$$

Since the WGS reaction is suppressed at low-temperature, [49] a continuous removal of H_2 from the reaction chamber is required to increase the methane conversion [50]. If the WSG reaction catalyst and H_2 separation membrane are integrated into one single unit, continuous separation of H_2 from the reactor will drive the equilibrium forward. A proton conducting membrane can be used with an external power source to extract hydrogen from the reforming side. Fig. 4b shows the

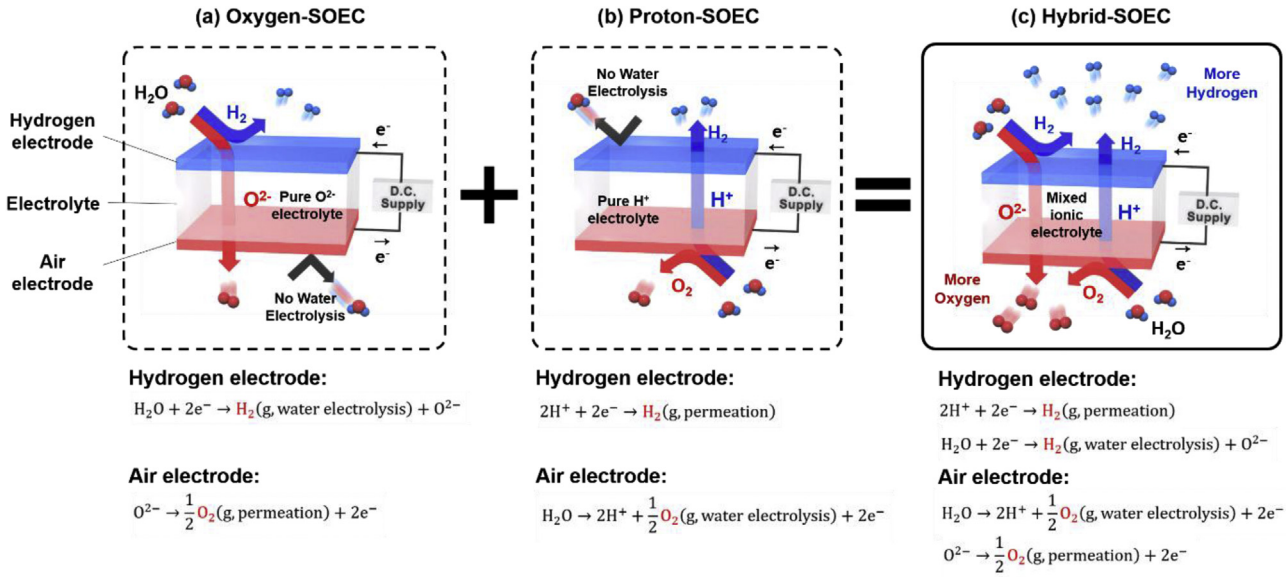

Fig. 3. Schematic illustration of the working principle for (a) Oxygen-SOEC, (b) proton-SOEC, and (c) Hybrid-SOEC systems. In the oxygen- and proton-SOEC systems (a and b), the water-electrolysis reaction occurs only at the one electrode. Meanwhile, water electrolysis can occur at both electrodes when mixed ion conducting electrolytes are used because of a counter-diffusion of electrolyzed ion species (O^{2-} and H^+) across the mixed ionic conducting electrolyte, reproduced with permission [34].

schematics of a proton-conducting solid electrolyte membrane.

Malerød-Fjeld et al. recently developed a membrane reactor with $BaZr_{0.8-x-y}Ce_xY_yO_{3-\delta}$ (BZCY) proton-conducting electrolyte sandwiched between two porous electrodes of BZCY and Ni that can separate hydrogen by applying 4.0 A cm^{-2}. At 800 °C, full methane conversion is achieved by removing hydrogen from other gases simultaneously with compression of hydrogen electrochemically up to 50 bar [51]. Furthermore, membrane reactors can be used for the hydrogenation and dehydrogenation of organic compounds [52–54]. Morejudo et al. demonstrated the dehydrogenation of methane to form aromatic compounds by using a co-ionic (proton and oxygen ion) conducting membrane and an externally applied current at 710 °C [55]. Dehydrogenation of ethane to ethylene was carried out using $BaZr_{0.4}Ce_{0.4}Y_{0.1}Yb_{0.1}O_{3-\delta}$ (BZCYYb) at 400 °C with an applied current density of 1 A cm^{-2} and achieved an ethylene selectivity close to 100% and a hydrogen generation rate of 0.448 mol cm^{-2} [56]. The H_2 permeable ceramic membrane reactor for non-oxidative CH_4 conversion (NMC) reaction is reported with Fe©SiO2 catalysts by Sakbodin et al. They have successfully increased the CH_4 conversion by the removal of H_2 from the NMC reactions without affecting the product selectivity and catalyst durability [57].

2.2.3. Ammonia synthesis

Ammonia synthesis by the Haber-Bosch process involves the reaction of gaseous nitrogen and hydrogen on the catalyst bed at high temperature and pressure (~500 °C, 150–300 bar). Since the ammonia formation reaction is exothermic at 500 °C (- 109 kJ mol^{-1}), ammonia formation increases with decreasing temperature. To obtain an industrially acceptable ammonia conversion rate, the high temperature is required to maintain a high conversion rate. However, the ammonia synthesis by the Haber-Bosch process is thermodynamically limited [58]. Electrochemical synthesis of ammonia using proton conducting membranes can overcome the thermodynamic limitations of the reversible reactions [59].

$$N_2 + 3H_2 \rightleftarrows 2NH_3 \quad (11)$$

Ammonia synthesis using proton conducting oxides typically involves the following steps, as shown in Fig. 4c:

1. Supply of H_2 at one electrode in the electrochemical cell.

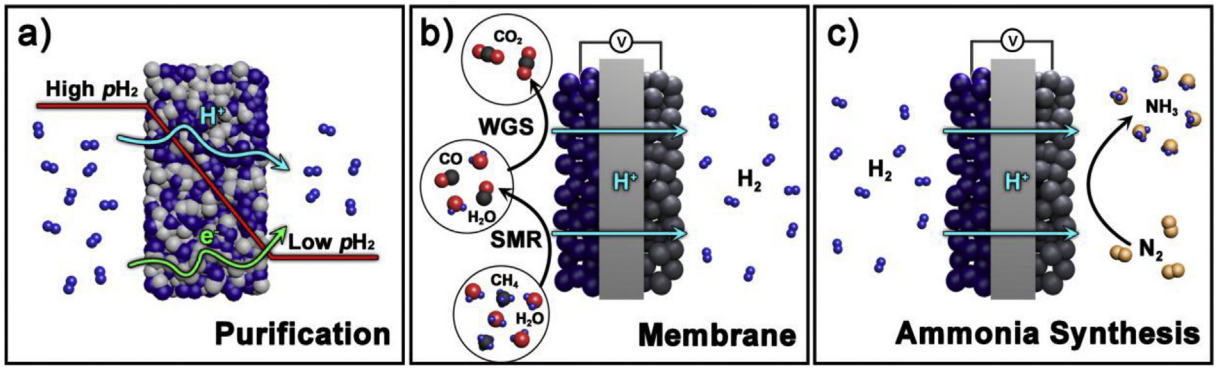

Fig. 4. (a) The design of ceramic proton conducting membranes with an electronic-protonic conduction. (b) Schematic illustration of the protonic membrane reformer. Methane (CH_4) is reformed with steam (H_2O) on the reaction side. H_2 is separated by protonic transport from the reaction side (with the lower partial pressure of hydrogen) to the hydrogen side ($pH_2 > pH_2$) and directly compressed as a result of applied voltage. Red, white and grey atoms represent O, H, and C, respectively. (c) Schematic illustration of proton conducting solid oxide cells employing proton-conducting electrolytes for electrocatalytic N_2 reduction. (For interpretation of the references to colour in this figure legend, the reader is referred to the Web version of this article.)

Table 1
Summary of representative single phase and dual phase ceramic proton conducting membranes for hydrogen separation.

Composition [Ref]	Temperature (°C)	Thickness (μm)	Flux (mL cm^{-2} min^{-1})	Feed gas/sweep gas
$BaZr_{0.8}Y_{0.15}Mn_{0.05}O_{3-\delta}$ [36]	900	900	0.03	Wet 50% H_2/He-wet Ar
$BaZr_{0.90}Fe_{0.10}O_{3-\delta}$ [37]	900	1150	0.75	20% H_2/inert Ar
$SrCe_{0.7}Zr_{0.2}Eu_{0.1}O_{3-\delta}$ [38]	900	30	0.23	100% dry H_2/inert
$BaCe_{0.95}Tb_{0.05}O_{3-\delta}$ [39]	850	15	0.53	50% H_2/N_2
Ni−$BaZr_{0.1}Ce_{0.7}Y_{0.1}Yb_{0.1}O_{3-\delta}$ [40]	900	44	1.12	Wet H_2/N_2
Ni−$BaZr_{0.1}Ce_{0.7}Y_{0.2}O_{3-\delta}$ [41]	900	266	0.80	H_2/100 ppm-N_2
Ni−$BaCe_{0.8}Y_{0.2}O_{3-\delta}$ [42]	900	80	0.2	3.8% H_2 in He/N_2
Ni−$BaCe_{0.95}Tb_{0.05}O_{3-\delta}$ [43]	900	10	0.91	50% H_2 in He/He
Ni−$BaZr_{0.7}Pr_{0.1}Y_{0.2}O_{3-\delta}$ [44]	950	400	0.01	wet 40% H_2/Ar
Ni−$BaZr_{0.1}Ce_{0.7}Y_{0.2}O_{3-\delta}$ [45]	900	30	0.33	80% H_2 in N_2/Ar
Ni−$Ba_{0.8}Ce_{0.35}Zr_{0.5}Tb_{0.15}O_{3-\delta}$ [46]	900	1500	0.07	25% H_2 25% CO_2 in N_2/Ar
$La_{5.5}WO_{11.25-\delta}$ − $La_{0.87}Sr_{0.13}CrO_{3-\delta}$ [47]	700	370	0.15	50% H_2 in Ar/N_2
$BaCe_{0.8}Y_{0.2}O_{3-\delta}$ − $Ce_{0.8}Y_{0.2}O_{2-\delta}$ [48]	900	1400	0.74	H_2 in He/Ar

2. Formation of protons at the electrode-electrolyte interface.
3. Proton conduction through the solid proton conducting membrane.
4. Reaction with N_2 to form ammonia at the other electrode.

An ideal proton conducting membrane should exhibit high proton conductivity; doped $SrCeO_3$, $BaCeO_3$, and $BaZrO_3$ exhibit appreciable proton conductivity for ammonia synthesis. Here, the ammonia synthesis rate using proton conducting oxides not only depends on the proton conductivity of the electrolyte membrane but also on the catalyst used in the electrode components. Table 2 summarizes representative proton conducting electrolytes and the rates of ammonia formation.

3. Materials

To enhance the performance of various electrochemical applications based on proton conducting oxides, many researchers have focused on developing electrochemically active materials that meet the essential requirements for the electrochemical cells. Electrochemical cells are basically composed of three components; electrolyte material for ion transfer and cathodic/anodic materials for redox reactions. Because of the operating similarities between fuel cells, electrolysis cells, and other electrochemical cells, these materials have been mainly developed for PCFC technologies, then applied to other applications such as electrolysis and electrochemical cells. Therefore, the overview of PCO materials in this section is composed of cathodic materials, electrolyte materials, and anodic materials. Also, different strategies for material development are described here based on the research progress of the PCFCs.

3.1. Cathodic materials

Generally, mixed ionic (O^{2-}) and electronic conductors (MIECs) have been used as the cathode material for conventional SOFC systems because of their excellent electron conductivity and catalytic activities for the oxygen reduction reaction (ORR). However, when the MIECs having poor proton conductivity are used as PCFC cathodes (Fig. 5a), the electrochemically active site is limited to the interface between cathode and electrolyte, because the protons should diffuse from the PCO electrolyte to the cathode material in order to generate electricity. This water formation at the interface of cathode and electrolyte could cause the first step to delamination if the formed water cannot be removed sufficiently. In order to operate the PCFC efficiently, the PCFC cathode material should have the property of electrochemical activity not only for O^{2-} and e^-, but also for H^+, (a triple conducting oxide, TCO), because the PCFC cathodic reaction involves these three species to extend the electrochemically active sites, effectively [70,71]. (Fig. 5b and c).

Uchida et al. [72] proposed basic elementary steps for the cathodic reaction considering not only the ORR, but also the water formation reaction in the PCFC. The elementary steps of the PCFC reaction based on proton transfer and reactions are proposed by *He* et al. and Poetzsch et al. [73,74].

The systematic development of TCOs is difficult because of the challenges of characterizing protonic behavior in the TCOs. To identify the protonic behavior of PCOs (i.e., proton conducting electrolyte materials), the EMF method is used through the measurement of open-circuit voltage (OCV) for concentration cells. For TCOs, However, it is difficult to measure the protonic properties by the EMF method because of their large electron conductivity. In addition, it is very complicated to analyze the thermodynamics and kinetics properties of TCOs, because not only H^+ but also O^{2-} and e^- simultaneously affects the cathodic performance of PCFCs. Despite these difficulties, extensive efforts have been devoted to increasing the electrochemical performance of the TCOs based on perovskite-related structures, such as simple perovskite ($ABO_{3-\delta}$, Fig. 6a), layered perovskite ($A'AB_2O_{5+\delta}$, Fig. 6b), and (c) Ruddlesden-Popper structure ($A_2BO_{4+\delta}$, Fig. 6c). Fig. 7 presents the representative non-ohmic resistances of PCFC single cells and representative single cell performances are listed in Table 3 with their specific configurations. According to Steele et al., the total area-specific resistivity (ASR) of cell components (electrolyte, anode, and cathode) should be below 0.50 Ω cm^2 to ensure high power densities, with targets of 1 kW dm^{-3} and 1 kW kg^{-1} [75]. Assuming that 30% of the total cell ASR is attributed to the electrolyte (*i.e.*, a typical value of 0.15 Ω cm^2), [3] the adequate performance is obtained from a PCFC provided the electrode's area specific resistance (ASR) is less than 0.35 Ω cm^2. In this section, the progress of cathodic materials is classified in accordance with three different strategies of material development; (1) finding MIEC materials having an electrocatalytic activity for proton reaction, (2) heavily doping transition metal into proton conducting oxides, and (3) mixing the proton conducting oxide with

Table 2
Summary of representative proton conducting electrolytes and the rates of ammonia formation.

Proton conductor membrane [Ref]	Temperature (°C)	NH_3 formation (mol s^{-1} cm^{-2})
$SrCe_{0.95}Yb_{0.05}O_{3-\delta}$ [58]	570	4.5×10^{-9}
$SrZr_{0.95}Y_{0.05}O_{3-\delta}$ [60]	450	6.2×10^{-2}
$BaCe_{1-x}Y_xO_{3-\delta}$ [61]	500	2.1×10^{-9}
$SrCe_{0.95}Yb_{0.05}O_{3-\delta}$ [62]	450	6.25×10^{-12}
$BaCe_{0.7}Zr_{0.2}Sm_{0.1}O_{3-\delta}$ [63]	500	2.7×10^{-9}
$Ba_{0.98}Ce_{0.8}Y_{0.2}O_{3-\delta}$ + 0.04 ZnO [64]	500	2.4×10^{-9}
$BaCe_{0.5}Zr_{0.3}Y_{0.16}Zn_{0.04}O_{3-\delta}$ [65]	450	4×10^{-9}
$BaZr_{0.7}Ce_{0.2}Y_{0.1}O_{2.9}$ [66]	620	1.7×10^{-9}
$BaCe_{0.85}Gd_{0.15}O_{3-\delta}$ [67]	500	5×10^{-9}
$BaCe_{0.85-x}Zr_xEr_{0.15}O_{3-\delta}$ [68]	450	3.27×10^{-9}
$BaCe_{0.85}Gd_{0.1}5O_{3-\delta}$ [69]	480	4.63×10^{-9}

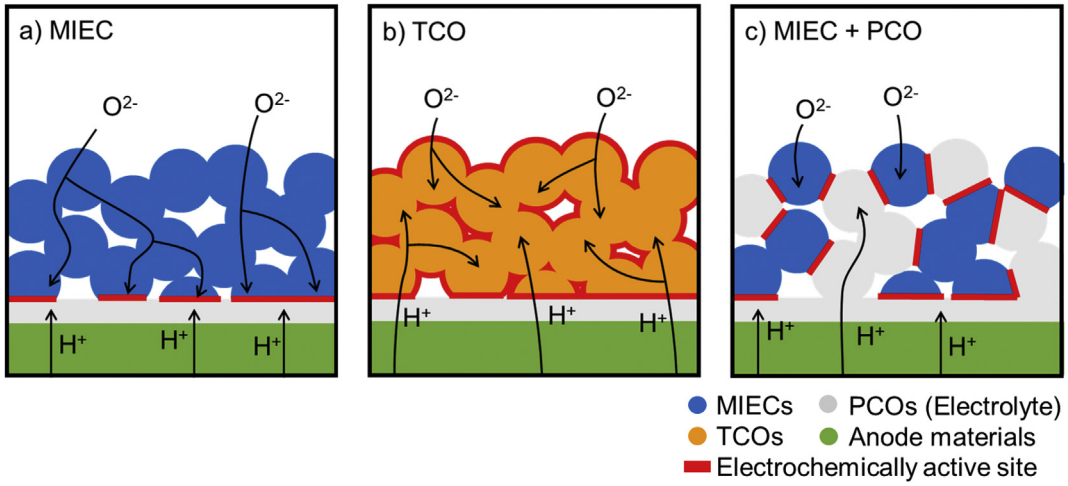

Fig. 5. Illustration of the electrochemically active sites for various cathode materials: (a) MIECs, (b) TCOs, and (c) mixtures of MIEC and PCO.

conventional MIEC materials.

3.1.1. MIEC materials having electro-catalytic activity for proton reaction

The first approach for the development of TCO is finding MIEC (O^{2-}/e^{-}) materials having a good electrochemical activity for the protonic reaction. Since the MIECs are already well-studied for the electro-catalytic mechanism of O^{2-} and e^{-}, many researchers have investigated to find protophilic MIECs for high-performance PCFCs. Grimaud et al. investigated the protonic properties of representative MIECs such as, $La_{0.6}Sr_{0.4}Fe_{0.8}Co_{0.2}O_{3-\delta}$ (LSCF), $Ba_{0.5}Sr_{0.5}Co_{0.8}Fe_{0.2}O_{3-\delta}$ (BSCF), $PrBaCo_2O_{5+\delta}$ (PBCO) and $Pr_2NiO_{4+\delta}$ (PNO) [90]. The highly oxygen deficient oxides (*i.e.*, BSCF and PBCO) present relatively high hydration properties compared to low oxygen-deficient oxide ($La_{0.6}Sr_{0.4}Fe_{0.8}Co_{0.2}O_{3-\delta}$), indicating that oxygen vacancy plays an important role in the proton uptake reaction from H_2O (*i.e.*, $V_O^{\bullet\bullet} + O_O^X + H_2O \rightarrow 2OH_O^{\bullet}$). The electrochemical measurements in this study show that PBCO and PNO could be considered as promising cathode materials for PCFC applications, and possible proton transfer could occur in these materials. For PBCO, BSCF, and PNO, electrode performances are improved with increasing pH_2O, and these electrochemical behaviors indicate that both O^{2-} and H^{+} related reactions participate in the PCFC electrochemical reaction.

Under practical PCFC operating conditions, layered perovskite materials have been considered as promising candidates because of their high catalytic activities for oxygen reduction reaction (ORR) and

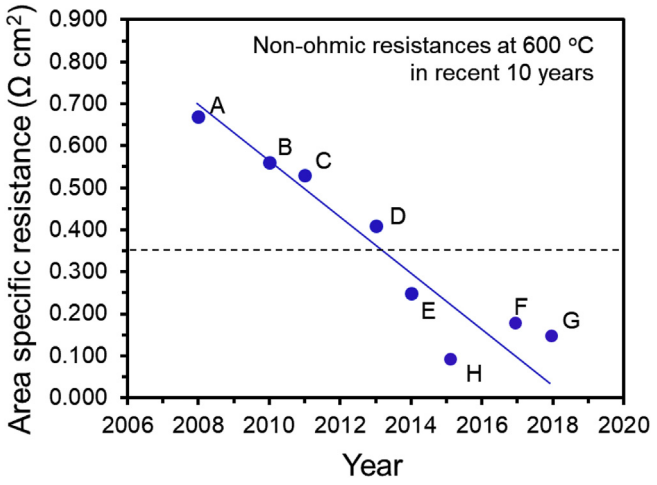

Fig. 7. Representative non-ohmic resistances of PCFC single cells at 600 °C in the last 10 years; A ($Sm_{0.5}Sr_{0.5}CoO_{3-\delta}$) [76], B($La_{0.6}Sr_{0.4}Fe_{0.8}Co_{0.2}O_{3-\delta}$-$Ba-Ce_{0.9}Yb_{0.1}O_{3-\delta}$) [77], C($La_{0.6}Sr_{0.4}Fe_{0.8}Co_{0.2}O_{3-\delta}$- $BaZr_{0.7}Pr_{0.1}Y_{0.2}O_{3-\delta}$) [78], D ($Sm_{0.5}Sr_{0.5}CoO_{3-\delta}$-$Ce_{0.8}Sm_{0.2}O_{2-\delta}$) [79], E ($NdBa_{0.5}Sr_{0.5}Co_{1.5}Fe_{0.5}O_{5+\delta}$) [80], F ($La_{0.6}Sr_{0.4}CoO_{3-\delta}$) [81], G ($PrBa_{0.5}Sr_{0.5}Co_{1.5}Fe_{0.5}O_{5+\delta}$) [25] and H($Ba-Co_{0.4}Fe_{0.4}Zr_{0.1}Y_{0.1}O_{3-\delta}$) [82].

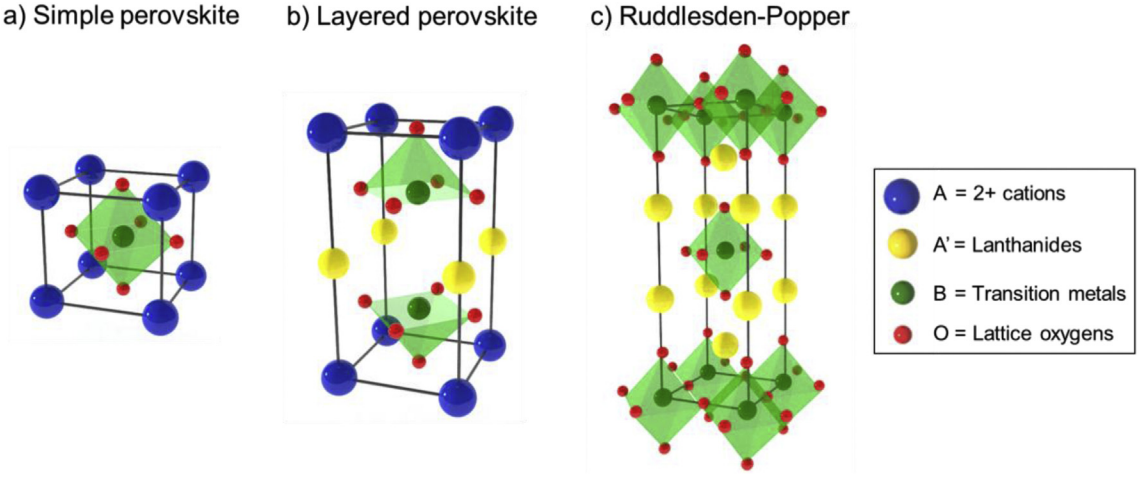

Fig. 6. Perovskite-related structures of representative triple conducting oxides (TCOs) for the PCFC cathode. (a) Simple perovskite ($ABO_{3-\delta}$), (b) layered perovskite ($A'AB_2O_{5+\delta}$), and (c) Ruddlesden-Popper structure ($A_2BO_{4+\delta}$).

Table 3
The electrochemical performances of PCFC single cells at 600 °C. ($Sm_{0.5}Sr_{0.5}CoO_{3-\delta}$ (SSC), $La_{0.6}Sr_{0.4}CoO_{3-\delta}$ (LSC), $Ce_{0.8}Sm_{0.2}O_{2-\delta}$ (SDC), $BaZr_{0.8}Y_{0.2}O_{3-\delta}$ (BZY), $BaZr_{0.1}Ce_{0.7}Y_{0.2}O_{3-\delta}$ (BZCY), $BaCe_{0.55}Zr_{0.3}Y_{0.15}O_{3-\delta}$ (BCZY3), $La_{0.6}Sr_{0.4}Fe_{0.8}Co_{0.2}O_{3-\delta}$ (LSCF), $BaZr_{0.7}Pr_{0.1}Y_{0.2}O_{3-\delta}$ (BZPY), $BaCe_{0.8}Sm_{0.2}O_{3-\delta}$ (BCS), $BaCe_{0.9}Yb_{0.1}O_{3-\delta}$ (BCYb), $BaZr_{0.7}Sr_{0.1}Y_{0.2}O_{3-\delta}$ (BZSY), $NdBa_{0.5}Sr_{0.5}Co_{1.5}Fe_{0.5}O_{5+\delta}$ (NBSCF), $BaCo_{0.4}Fe_{0.4}Zr_{0.1}Y_{0.1}O_{3-\delta}$ (BCFZY), $BaZr_{0.1}Ce_{0.7}Y_{0.1}Yb_{0.1}O_{3-\delta}$ (BZCYYb), $PrBa_{0.5}Sr_{0.5}Co_{1.5}Fe_{0.5}O_{5+\delta}$ (PBSCF), $Ba_{0.5}Sr_{0.5}Co_{0.8}Fe_{0.2}O_{3-\delta}$ (BSCF), and $BaZr_{0.4}Ce_{0.4}Y_{0.1}Yb_{0.1}O_{3-\delta}$ (BZCYYb4411)).

Year [Ref]	Cathode	Electrolyte (thickness)	Anode	Ohmic resistance (Ω cm^2)	Non-ohmic resistance (Ω cm^2)	Maximum power density (mW cm^{-2})
2012 [83]	SSC-SDC	BZY (25 μm)	Ni-BZCY	3.240	1.980	55
2009 [84]	BCB	BZCY (25 μm)	Ni-BZCY	0.670	1.600	125
2014 [85]	BZCY-SSC	BZCY (20 μm)	Ni-BZCY	0.357	1.318	240
2010 [86]	SSC	BZY (20 μm)	Ni-BZCY	1.400	1.300	70
2010 [87]	LSCF-BZPY	BZPY (20 μm)	Ni-BZY	1.330	1.300	82
2008 [76]	SSC	BCS (70 μm)	Ni-BCS	0.100	0.670	420
2010 [77]	LSCF-BCYb	BZY (20 μm)	Ni-BZY	1.850	0.560	112
2011 [78]	LSCF-BZPY	BZPY (12 μm)	Ni-BZY	0.530	0.530	163
2013 [79]	SSC-SDC	BZSY (12 μm)	Ni-BZSY	0.460	0.410	290
2014 [80]	NBSCF	BZCYYb (15 μm)	Ni-BZCYYb	0.128	0.248	700
2015 [82]	BCFZY	BZCYYb (20–30 μm)	Ni-BZCYYb	0.290	0.086	650
2018 [88]	BSCF	BCZY3 (5 μm)	NiO-BCZY3	0.090	0.090	1302
2018 [89]	LSC	BCZY3 (1 μm)	NiO-BCZY3	0.060	0.210	1125
2018 [25]	PBSCF without PLD layer	BZCYYb 4411 (15 μm)	Ni-BZCYYb 4411	0.178	0.148	873
2018 [25]	PBSCF with PLD layer	BZCYYb 4411 (15 μm)	Ni-BZCYYb 4411	0.088	0.139	1098

protonic reaction. This family of layered perovskite compounds has the general formula $AA'B_2O_{5+\delta}$, where A is a trivalent lanthanide ion (Ln = Pr, Nd, Sm, and Gd), A′ is Ba^{2+} or Sr^{2+}, and B is a first-row transition metal ion or a mixture thereof. The layered perovskite consists of two layers with the alternating stacking of … |A'O|BO_2|AO_δ|BO_2| … For example, PCFC single cells having $LnBaCoO_{5+\delta}$ (Ln = Pr, Sm, Gd) cathodes exhibits a considerable maximum power density (MPD) value of 266–382 mW cm^{-2} at 700 °C [91–93]. Numerous work has been reported in the literature in order to further enhance the electrochemical performance and stabilities by doping several transition metals into the layered perovskite materials [96,97]. Among those possible dopants, Sr^{2+} doping into the cobalt site of SBCO and PBCO shows significantly higher MPD values of 520–533 mW cm^{-2} with low polarization resistance of 0.080–0.120 Ω cm^2 at 700 °C [94,95]. The electrochemical performance of $GdBaCoFeO_{5+\delta}$ (GBCO) cathode also effectively increase with Fe doping into the cobalt site. The GBCO shows a polarization resistance and MPD of 0.011 Ω cm^2 and 482 mW cm^{-2} [97]. Recently, the excellent electrochemical performance of PCFC single cells was achieved by the co-substitution of cobalt and iron into $LnBaCoO_{5+\delta}$ (Ln = Pr, Nd). $NdBa_{0.5}Sr_{0.5}Co_{1.5}Fe_{0.5}O_{5+\delta}$ (NBSCF) shows excellent electrochemical performance with a low polarization resistance of 0.128 Ω cm^2 and high MPD of 690 mW cm^{-2} even at 600 °C under practical PCFC operating condition. Also, $PrBa_{0.5}Sr_{0.5}Co_{1.5}Fe_{0.5}O_{5+\delta}$ (PBSCF) presents a remarkable MPD of 890 mW cm^{-2} at 600 °C [25]. A dense layer of PBSCF, fabricated by pulsed laser deposition (PLD) enhances the contact between cathode and electrolyte, considerably reducing the ohmic losses. The application of a PLD layer resulted in a remarkable power density of 1098 mW cm^{-2} at 600 °C.

Concerning the simple perovskite materials, Lin et al. reported that the $Ba_{0.5}Sr_{0.5}Co_{0.8}Fe_{0.2}O_{3-\delta}$ (BSCF) presents an attractive MPD of ~550 mW cm^{-2} at 700 °C with BCY electrolytes, but an 1100 °C fired cathode shows a much lower MPD of only ~225 mW cm^{-2} at 700 °C because of the cation diffusion of BSCF [98]. These results imply that the sintering temperature of the cathode layer should be carefully controlled to prevent the formation of secondary phase and to obtain good adhesion between electrolyte and cathode. A low polarization resistance of 0.07 Ω cm^2 is achieved from the BZY cell at 600 °C with PBCO-based nanoparticle cathode [99].

The cathodic polarization of cobalt-free materials has been investigated for PCFCs, but these materials present relatively low power densities; $La_{0.7}Sr_{0.3}MO_{3-\delta}$ (M = Fe, Mn and Co) [100], $BaCe_{0.5}Fe_{0.5}O_{3-\delta}$ (BCF) [101], $BaCe_{0.5}Bi_{0.5}O_{3-\delta}$ (BCB) [84], and $NdBaFe_{2-x}Mn_xO_{5+\delta}$ (NBFM) [102].

3.1.2. Triple conducting oxides based on heavily doping of transition metal into proton conducting oxides

To develop electrochemically active TCOs, various altervalent elements are doped into pure proton conducting oxides (*i.e.*, BZO or BCO) to enhance their electrochemical activity for O^{2-} and e^-. For example, many altervalent ions are doped into the B-site of PCO to increase oxygen-ion kinetics, and Mukundan et al. reported on the substitution of Pr and Gd into the B-site of $BaCeO_{3-\delta}$ for triple conducting electrodes [103]. In a later study, they found that this compound presents a minor protonic contribution with p-type conduction under a wet atmosphere [104]. Fabbri et al. also tried to increase the p-type conductivity of $BaCeO_{3-\delta}$ by using a multivalent dopant, such as Sm, Eu, and Yb [105]. Transport numbers for $BaCe_{0.9}Yb_{0.1}O_{3-\delta}$ (BCYb) were calculated from an established defect model by measuring the conductivities at different oxygen partial pressures, and BCYb shows a mixed ionic and hole conduction above 600 °C.

Merkle et al. investigated a complex behavior of triple conducting properties with respect to equilibrium thermodynamics and diffusion kinetics after pH_2O and pO_2 [14,106,107]. According to the defect chemistry model, the protonic reaction after a pH_2O increase changes from predominantly water uptake in materials ($H_2O + O_O^X + V_O^{\bullet\bullet} \rightarrow 2OH_{O,}^{\bullet}$ hydration reaction) to hydrogen incorporation ($H_2O + 2O_O^X + 2\,h^{\bullet} \rightarrow 2OH_{O,}^{\bullet}$ hydrogenation reaction).

Transition-metal cation (*i.e.*, Co and Fe) doped $BaZrO_{3-\delta}$ is identified as a TCO material [108]. $BaCo_{0.4}Fe_{0.4}Zr_{0.2}O_{3-\delta}$ (BCFZ) presents a promising electrochemical performance with high stability on $BaZr_{0.1}Ce_{0.7}Y_{0.1}Yb_{0.1}O_{3-\delta}$ (BZCYYb) electrolyte single cells. The activation energy of a BCFZ cathode is identified as 76 kJ mol^{-1} which is significantly lower than that of LSCF cathode material (138 kJ mol^{-1}). Recently, O'Hayre et al. reported that readily processed PCFC with $BaCo_{0.4}Fe_{0.4}Zr_{0.1}Y_{0.1}O_{3-\delta}$ (BCFZY0.1) cathode material infiltrated into the $BaCe_{0.6}Zr_{0.3}Y_{0.1}O_{3-\delta}$ (BCZY63) backbone [82]. The Ni-BZCYYb/BZCYYb/BZY63-BCFZY0.1 single cell presents an excellent maximum power density of 455 mW cm^{-2} at 500 °C.

3.1.3. Mixture of MIECs and proton conducting oxides

Many studies have been made on composite cathodes containing mixtures of proton conducting electrolyte and MIEC materials to extend the triple phase boundaries (TPBs) where the cathodic reactions occur [1]. The electrochemical performance of both single-phase LSCF and LSCF- $BaCe_{0.9}Yb_{0.1}O_{3-\delta}$ composite cathodes (1:1 wt ratio) were

carefully characterized by electrochemical impedance spectroscopy (EIS) analysis [109]. The LSCF-$BaCe_{0.9}Yb_{0.1}O_{3-\delta}$ composite cathode exhibits relatively higher performance than a single-phase LSCF cathode. This result could imply that the cathodic reaction occurs only between the electrolyte and the cathode for the single-phase LSCFs, while the electrochemical reaction area is effectively extended by adding the proton conducting oxide, $BaCe_{0.9}Yb_{0.1}O_{3-\delta}$. The Ni-BZCYYb/BZCYYb/BZCY-LSCF single cell exhibits an excellent maximum power density of $\sim 660\,mW\,cm^{-2}$ at 650 °C. Also, other composite cathode materials have been investigated in many studies, [110–112] but these are not covered here to avoid duplication of previous reviews. (The comprehensive overview of PCFC composite cathodes can be found in the reference [1]) These findings imply that electrochemically active MIEC and PCO materials must be used in an optimized ratio without chemical reaction between them. Also, the TPB can be changed depending on the particle size of each of MIEC and PCO; the effect of morphological changes on the electrochemical performance of composites needs to be investigated.

3.2. Electrolyte materials

In the early 1980s, Iwahara et al. first showed proton conduction in $SrCeO_3$, $BaCeO_3$, and other perovskite related oxides at relatively high temperature in a humidified hydrogen atmosphere. Proton conduction is based on the existence of proton defects at a moderate temperature and dissociative absorption of water, which requires the presence of oxygen vacancies. The protonic defects are formed from the dissociation of water into proton and hydroxide ion; the proton forms a covalent bond with the lattice oxygen and the hydroxyl ion fills the oxygen vacancy. This process can be written according to Kroger-Vink notation as,

$$H_2O + O_O^X + V_O^{\cdot\cdot} \leftrightarrow 2OH_O^{\cdot} \quad (12)$$

It is widely accepted that proton diffusion in perovskite-type oxides proceeds in two basic steps [113]. As illustrated in Fig. 8, in a reorientation step (Step 1), the OH group is bent towards the adjacent oxygen ion, so that the bond length decreases the energetic barrier for proton transfer and the protons can be transferred by the breaking/formation of hydrogen bonds. In a proton transfer step (Step 2), due to the presence of protonic defects, the proton migrates by proton hopping between neighboring oxide ions (O_O^X). The proton can hop from one oxygen ion to another by breaking the weak O—H bonds and forming new O—H bonds with the neighboring oxygen ions by an approach of the two oxygen [6].

The probable long-range proton conducting pathways can be influenced by the distortions of the perovskite structure, chemical perturbation induced by cation dopant, and proton-dopant association. Any change in crystal symmetry that deviates from the ideal cubic structure is detrimental to proton conduction. The most common example is Y doped $BaCeO_3$ and Y doped $SrCeO_3$ [113]. Among these two cerates, Y-doping in $SrCeO_3$ promotes orthorhombicity compared to Y doped $BaCeO_3$, which leads to easier proton migration in Y doped $BaCeO_3$. Proton – dopant association (*i.e.*, proton trapping) is another serious issue to be considered in proton conducting electrolytes [114]. Because of their opposite charge, positively charged protons and negatively charged dopants usually attract each other. Proton nuclear magnetic resonance experiments on Y doped $BaZrO_3$ indicate that the proton must overcome barriers for conduction, as the proton diffusion coefficient decreases. In other words, one of these normal sites is the barrier to escape trapping and a small barrier to long-range conduction. In the Y-doped $BaZrO_3$ case, incorporated protons must overcome the association energy of $9\,kJ\,mol^{-1}$ (proton trapped at dopant site), as well as the general activation energy of $16\,kJ\,mol^{-1}$ for the long-range transport [24]. Kreuer et al. comprehensively discussed the chemical and structural parameter determining the formation and mobility of protonic defects along with the effect of various dopants [115,116]. Islam et al. found that there was an increase in the activation energy for proton diffusion with increasing dopant content, which may be correlated to the increase in oxygen basicity and barrier for proton transfer [114].

Doped barium cerate and strontium cerate perovskite-type oxides showed the highest proton conductivity among all the high-temperature proton conductors. However, in terms of stability, they easily react with water vapor and acidic gases like CO_2 and SO_2 to form hydroxides and carbonates respectively. For instance, 10% Sm-doped barium cerate decomposed when exposed to CO_2 above 400 °C. Gopalan and Virkar [117] reported the thermodynamic stability of $BaCeO_3$ in a CO_2 atmosphere according to Equation (13) and Gd-doped $BaCeO_3$ decomposed when exposed to water vapor (pH_2O of 1 atm) below 400 °C [37] according to Equations (13) and (14) [118].

$$BaCeO_3 + CO_2 \rightarrow CeO_2 + BaCO_3 \quad (13)$$

$$BaCeO_3 + H_2O \rightarrow CeO_2 + Ba(OH)_3 \quad (14)$$

Since protonic ceramics fuel cells (PCFCs) operate under extreme conditions, barium base electrolyte shows degradation which limits its application in the PCFCs. To overcome the problem of poor chemical stability, dopants have been introduced to stabilize the barium cerate and should not affect the high proton conductivity. Matsumoto et al. reported the relationship between the ionic conductivity and chemical stability by doping the various size of cations [119]. They found that the replacement of Ce^{+4} in barium cerate with larger ionic radius dopants increases the chemical stability.

Doped barium-zirconates, on the other hand, display high chemical stability in water vapor and CO_2 atmosphere. The primary disadvantage of $BaZrO_3$ based proton conductors is poor sinterability to fabricate dense membranes and high resistance for the proton conduction at the grain boundaries. Numerous studies have been reported in the literature to improve the sinterability of $BaZrO_3$ by adding sintering aids. The use of $LiNO_3$ has been reported to fabricate a dense BZY20 electrolyte

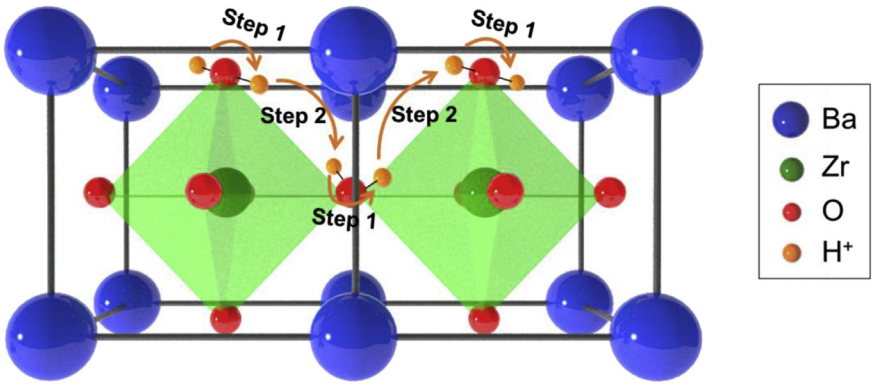

Fig. 8. Schematic illustration of the reorientation (Step 1) and proton transfer (Step 2) pathways. The small orange balls represent the minimum energy position of the proton, and they are equivalent due to the symmetry of the crystal. (For interpretation of the references to colour in this figure legend, the reader is referred to the Web version of this article.)

(96.5% of the theoretical value) after sintering at 1600 °C [120]. A total conductivity of 4.45×10^{-3} S cm^{-1} at 600 °C was reported in wet Ar atmosphere. Chemical analysis shows that the Li-additive evaporates during the sintering process. Also, the use of non-volatile sintering aids decreases the electrical conductivity of BZY probably due to sintering aids entering the perovskite structure. Meanwhile, a sintering behavior of BZY20 was investigated with other sintering aids and it has been reported that the nickel oxide is effective for producing dense and high conductivity proton conducting oxides [121]. Li et al. reported that the densification of electrolytes could be promoted by using an anode material having high shrinkage properties [122]. A significant improvement in conductivity has also been reported with epitaxially oriented barium zirconate thin films grown by pulsed laser deposition [123,124].

Additionally, several works have focused on the development of chemically stable and highly conductive electrolytes by the preparation of solid solutions of $BaZrO_3$ and $BaCeO_3$ [125]. Since both $BaZrO_3$ and $BaCeO_3$ are mutually soluble, it is possible to prepare a chemically stable electrolyte with the desired proton conductivity by controlling a fraction of Zr in $BaZrO_3$ with Ce. Increasing the Ce content in $BaZrO_3$ commonly resulted in improving the overall conductivity, sinterability, and decreasing the chemical stability in CO_2 and water vapor. Based on this approach, the chemical stability of $BaCe_{0.9-x}Zr_xY_{0.1}O_3$ against CO_2 and water vapor under experimental conditions indicated that the material is stable when the amount of Zr contents is larger than 0.4. In reality, a solid solution of $BaZrO_3$ - $BaCeO_3$ often results in a tradeoff between the proton conductivity and chemical stability of the electrolyte. Besides the composition of solid solutions, synthesis of $BaZrO_3$ - $BaCeO_3$ solid solutions also influences the chemical stability. Powders prepared by a solid state reaction method is more stable than powders prepared by a citrate combustion method when treated with 3% CO_2 at 600 °C for seven days [126]. In addition to the solid solutions, doping strategies for optimized chemical stability and electrical conductivity were also carefully examined [127]. Doping with In, Gd, and Nd has been reported to show some improvement in the chemical stability and proton conductivity of $BaZrO_3$—$BaCeO_3$ solid solutions [128–130]. $BaZr_{0.1}Ce_{0.7}Y_{0.1}Yb_{0.1}O_3$ (BZCYYb) electrolyte developed by substituting 10% Y and 10% Yb in $BaZrO_3$ - $BaCeO_3$ solid solutions at Ce sites, showed much-improved chemical stability, and sinterability compared with $BaCeO_3$ [131]. Interestingly, the work showed a transition of an ionic conduction in BZCYYb materials from majority proton conduction to oxygen ion conduction with increasing temperature. The effect of co-doping in Ce sites is not fully straightforward, but the experimental measurements show that the conductivity of BZCYYb materials is higher than the conductivities of materials with an individual dopant at Ce sites. This mixed ionic property is due to the relatively high oxygen vacancy concentration formed by double doping of 3^+ (Y and Yb) cations into the Ce^{4+} site in the intermediate temperature range (750–850 °C). Also, transference number measurements in different (H_2/H_2O and O_2/H_2O) concentration cells confirm that the conductivity of the BZCYYb electrolyte is mixed ionic. The significant role of oxygen ion and proton conduction dictates that water can be electrolyzed and formed at both the air and fuel electrodes. This makes the BZCYYb material useful because it increases the efficiency of SOE as well as it allows the internal reforming of hydrocarbons at the fuel electrode [34]. A significant improvement in chemical stability and ionic conductivity has been reported for $BaZr_{0.4}Ce_{0.4}Y_{0.1}Yb_{0.1}O_3$ fabricated using a ratio of Zr:Ce = 1:1, whereas previous works have been using a 1:7 composition. The BZCYYb4411 shows a great chemical stability of BZCYYb electrolyte in a 100% CO_2 atmosphere [25]. Recently, anode assisted method for a single cell is proposed a for densifying PCO electrolyte [121]. An et al. reported an exceptional high power density of 1.3 W cm^{-2} at 600 °C in a large scale (5×5 cm^2) [88].

While some materials have high ionic conductivity, their applicability as the electrolyte in fuel cells is limited when exposed to hydrogen. Zhou et al. developed an electron doping strategy and demonstrated $SmNiO_3$ perovskite as an electrolyte material for PCFCs. When SNO is exposed to hydrogen, electrons are doped into SNO via hydrogen incorporation by the reduction of Ni^{3+} ions to Ni^{2+} ions; no oxygen vacancies are formed upon reduction.

$$Ni^{3+} + O_O^X + ½H_2 \leftrightarrow Ni^{2+} + OH_O^{\cdot} \quad (15)$$

Remarkably, a high ionic conductivity was archived at 500 °C with low activation energy (~0.3 eV) compared to several other proton-conducting electrolyte materials. Although electron doping strategies open a new direction for the advancement of proton conducting electrolytes, their practical application for fuel cell fabrication is limited due to expensive fabrication techniques.

In an alternative to cerates and zirconates related materials, several other oxides have been shown, by desirable proton conductivity to be suitable for use as electrolyte materials for PCFCs. Among the other stable proton conducting materials, most promising compounds are described as acceptor doped rare-earth orthoniobates and orthotanthalates with the general formula $RE_{(1-x)}A_xMO_4$ (where RE = La, Gd, Nd, Te, Er, Y; M = Nb, Ta and A = Ca, Sr, Ba); with x usually varies from 0.01 to 0.05. Rare-earth orthoniobates exist in two different polymorphs; a high-temperature tetragonal Scheelite-type structure and a low-temperature monoclinic Fergusonite-type with different activation energies for proton conduction 0.73–0.83 eV and 0.52–0.62 eV, respectively [132,133]. $La_{0.99}Ca_{0.01}NbO_4$ has been reported to have conductivity close to 0.001 S cm^{-1} at 950 °C under 2.5% H_2O [118] and ~2×10^{-4} S cm^{-1} was reported at 800 °C for $La_{0.99}Ca_{0.01}TaO_4$. To achieve a reasonable fuel cell performance, the electrolyte thickness must be decreased towards the 1 μm range along with other obstacles. Also, some other perovskite-related materials, such as fluorite-related materials, and pyrochlore related structures, show considerable proton conduction with good chemical stability. Their practical application as electrolytes in PCFCs are still limited due to poor conductivity; because the electrolyte component requires an ohmic resistance of less than 0.15 Ω cm^2 to the total area specific resistance of fuel cells [118].

3.3. Anodic and functional materials

3.3.1. Anodic properties in PCFCs

Most PCFCs use composite anodes of Ni with the proton conducting electrolytes to increase the number of electrochemically active sites for fuel oxidation, improve intimate contact with the electrolyte, and increase durability during cell operations [134,135]. For example, Ni—$BaZr_{0.1}Ce_{0.7}Y_{0.1}Yb_{0.1}O_{3-\delta}$ (BZCYYb) composites have been investigated as PCFC anodes because of their excellent catalytic activity and high sulfur and coking tolerance [136]. Comparing with the conventional oxygen conducting SOFCs, the more theoretical value of OCV can be achieved in PCFC operating condition because water formation reaction occurs at the cathode and thus PCFCs can avoid dilution of fuels [137]. In addition, PCFCs are less affected by the porosity of anode compared to oxygen ion conducting SOFCs because PCFC anode requires less porosity for water removal. For example, the performance of the Ni-YSZ cermet anode increases with increasing porosity. Thus pore formers are needed to increase the porosity [138]. In contrast, the lowest porosity (37 vol.%) of Ni-BZCYYb prepared without pore former shows the highest performance (1.2 W cm^{-2} at 750 °C) under fuel cell operating conditions [139].

3.3.2. Functional materials for carbon coking and sulfur poisoning tolerance

Ceramics fuel cells use nickel-based cermet anodes that exhibit high activity for the electrocatalytic oxidation of hydrogen, high electronic conductivity, and good compatibility with electrolytes [134,140]. However, under hydrocarbon fueled operating condition, carbon coking occurs on the surface of nickel-based anodes, leading to reduced electrochemical active sites and degraded fuel cell performance

[141,142]. In addition, hydrogen sulfide (H_2S) in reformed hydrocarbon fuels could cause serious sulfur poisoning because of sulfur adsorption on the nickel surface, even in parts per million (ppm) levels [143–145]. Accordingly, alternative anode materials such as Ni-free ceramic anodes have been developed for direct hydrocarbon fuel cells [146–148]. Although these alternative anode materials have demonstrated some improved coking and sulfur tolerance in hydrocarbon fuels, [149,150] they have poor electrochemical activity, low electrical conductivity, and insufficient compatibility with an electrolyte at high temperatures [151,152].

To maintain the high electrochemical performance of Ni-based anodes while enhancing the tolerance to carbon coking and sulfur poisoning, a surface modification of Ni-based anodes has been widely researched. For example, proton conducting materials such as BZCYYb [153], $BaZr_{1-x}Y_xO_3$ [154], $BaZr_{1-x}Yb_xO_3$ [155], and BaO [156] have shown excellent carbon coking tolerance and sulfur tolerance due to their high water uptake property. The adsorbed water on the proton conducting materials reacts with adsorbed carbon and sulfur on the Ni surface to produce CO and SO_2, respectively, which can be expressed by the following reactions:

$$C^*_{Ni} + 2H_2O_{proton} \rightarrow CO_2 + Ni + 2H_2 \quad (16)$$

$$S^*_{Ni} + 2H_2Oproton \rightarrow SO_2 + Ni + 2H_2 \quad (17)$$

where H_2O_{proton} refers to adsorbed water on the proton material surface, C^*_{Ni} refers to carbon adsorbs on the Ni surface, and S^*_{Ni} refers to sulfur adsorbed on the Ni surface.

In this regard, various methods have been reported to enhance the tolerance by surface modification of Ni-YSZ with the proton conductive materials. Sengodan et al. modified the Ni-YSZ anode by the infiltration of $BaZr_{0.1}Ce_{0.7}Y_{0.1}Yb_{0.1}O_{3-\delta}$ (BZCYYb) to enhance sulfur tolerance [158]. The BZCYYb particles are mainly located on the Ni surface by single-step infiltration, which demonstrates stable performance in a significant concentration of sulfur over 500 h. For improving carbon coking tolerance, Liu et al. reported a multi-functional catalyst layer derived from NiO-YSZ with $BaCO_3$. The BaO nanoparticles on the Ni surface and $BaZr_{1-x}Y_xO_{3-\delta}$ (BZY) on YSZ are formed from the surface modification, improving both the oxidation of reformed fuels and the reforming of octane [156]. For improving sulfur tolerance, Kwon et al. reported a $BaZrO_3$ (BZO) modified NiO-YSZ anode fabricated by co-sintering NiO-YSZ and $BaCO_3$ at high temperature [157]. As shown in Fig. 9, BZO modified NiO-YSZ has NiO, YSZ, and BZO phases that are adjacent to each other, and the adsorbed water on the BZO surface removes sulfur on the Ni surface through producing SO_2 and H_2. The anode supported cell with the BZO modified Ni-YSZ anode presents noticeably stable performance over 100 h in humidified H_2 containing 100 ppm H_2S compared to without surface modification. Recently, Duan et al. reported an excellent performance and exceptional durability of PCFC operation using 11 different fuels at a temperature range of 500–600 °C [159]. They reported that major degradation factors (e.g., carbon coking and sulfur poisoning) could be moderated using proton conducting oxides having good water uptake properties.

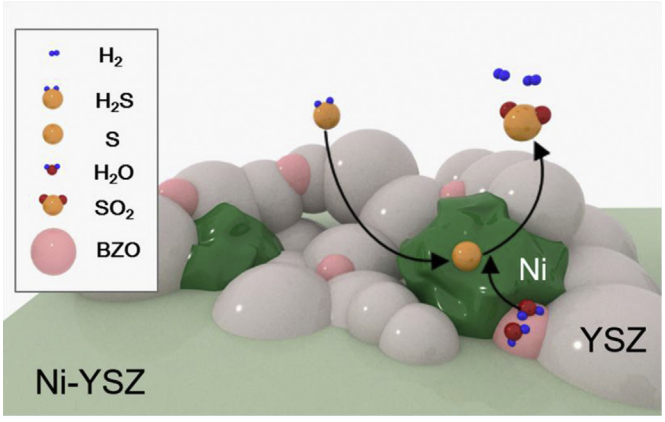

Fig. 9. Schematic illustration of the sulfur removal process for the BZO modified Ni-YSZ anode under sulfur contaminated H_2 fuel, reproduced with permission [157].

4. Conclusion

In this review, the recent progress of proton conducting oxides and electrode materials is summarized for protonic electrochemical devices such as fuel cells, electrolyzes, membrane reactors and hydrogen separation membrane. In order to fully implement the advanced proton conductors into the energy conversion and storage devices, there are still a lot of concerns should be resolved. One of the most vital problem in a protonic ceramic fuel cell is the sluggish kinetics of oxygen/proton electrochemistry with high polarization resistance. The use of triple conducting oxides has shown very promising catalytic activity for oxygen reduction reaction and protonic reaction and exceptional power density under intermediate temperature operating conditions. For proton conducting electrolyte membrane besides addressing their conventional issues such as chemical stability and sinterability, it requires to develop a ceramic processing technique that shows high protonic conductivity with low grain boundary resistance. Optimization of cell design, package design, and membrane design are additional concerns that should be resolved before practical applications. With advances in material science and deep understanding of the PCOs, significant breakthroughs are expected in promising protonic energy conversion and storage applications beyond current technology in the near future.

Declarations of interest

None.

Acknowledgments

This research was supported by the Korea Institute of Energy Technology Evaluation and Planning (KETEP) and the Ministry of Trade, Industry & Energy (MOTIE) of the Republic of Korea (No. 20173010032120), and the Mid-career Researcher Program through the National Research Foundation of Korea, funded by the Ministry of Science, ICT and Future Planning (NRF- 2018R1A2A1A05077532).

Nomenclature and Abbreviation

ASR	area specific resistance, Ω cm^2
ECS	energy conversion and storage
EMF	electromotive force
H	Enthalpy
LT-SOFC	low-temperature solid oxide fuel cell
MIECs	mixed ionic (O^{2-}) and electronic conductors
MPD	maximum power density, W cm^{-2}
MSR	methane steam reforming
NMC	non-oxidative methane conversion
ORR	oxygen reduction reaction
PCEC	protonic ceramic electrolysis cell
PCFC	protonic ceramic fuel cell
PCO	proton conducting oxide
PLD	pulsed laser deposition
SOFC	solid oxide fuel cell
TCO	triple conducting oxide
WGS	water gas shift reaction
μ	chemical potential, J mol^{-1}
ΔG	Gibbs free energy, J mol^{-1}

References

[1] Fabbri E, Bi L, Pergolesi D, Traversa E. Towards the next generation of solid oxide fuel cells operating below 600 °C with chemically stable proton-conducting electrolytes. Adv Mater 2012;24:195–208.
[2] Iwahara H, Asakura Y, Katahira K, Tanaka M. Prospect of hydrogen technology using proton-conducting ceramics. Solid State Ionics 2004;168:299–310.
[3] Brett DJ, Atkinson a, Brandon NP, Skinner SJ. Intermediate temperature solid oxide fuel cells. Chem Soc Rev 2008;37:1568–78.
[4] Iwahara H, Esaka T, Uchida H, Maeda N. Proton conduction in sintered oxides and its application to steam electrolysis for hydrogen production. Solid State Ionics 1981;3–4:359–63.
[5] Iwahara H. Proton conducting ceramics and their applications. Solid State Ionics 1996;86–88:9–15.
[6] Kreuer K-D. Proton conductivity: materials and applications. Chem Mater 1996;8:610–41.
[7] Mahato N, Banerjee A, Gupta A, Omar S, Balani K. Progress in material selection for solid oxide fuel cell technology: a review. Prog Mater Sci 2015;72:141–337.
[8] Wachsman ED, Lee KT. Lowering the temperature of solid oxide fuel cells. Science 2011;334:935–9.
[9] Kreuer KD. Proton-conducting oxides. Annu Rev Mater Res 2003;33:333–59.
[10] Norby T. Solid-state protonic conductors: principles, properties, progress and prospects. Solid State Ionics 1999;125:1–11.
[11] Fabbri E, Pergolesi D, Traversa E. Materials challenges toward proton-conducting oxide fuel cells: a critical review. Chem Soc Rev 2010;39:4355.
[12] Malavasi L, Fisher C a J, Islam MS. Oxide-ion and proton conducting electrolyte materials for clean energy applications: structural and mechanistic features. Chem Soc Rev 2010;39:4370–87.
[13] Kochetova N, Animitsa I, Medvedev D, Demin A, Tsiakaras P. Recent activity in the development of proton-conducting oxides for high-temperature applications. RSC Adv 2016;6:73222–68.
[14] Poetzsch D, Merkle R, Maier J. Proton uptake in the H^+-SOFC cathode material $Ba_{0.5}Sr_{0.5}Fe_{0.8}Zn_{0.2}O_{3-\delta}$: transition from hydration to hydrogenation with increasing oxygen partial pressure. Faraday Discuss 2015;182:129–43.
[15] Choi S, Yoo S, Kim J, Park S, Jun A, Sengodan S, et al. Highly efficient and robust cathode materials for low-temperature solid oxide fuel cells: $PrBa_{0.5}Sr_{0.5}Co_{2-x}Fe_xO_{5+\delta}$. Sci Rep 2013;3:2426.
[16] Tarancón A, Skinner SJ, Chater RJ, Hernández-Ramírez F, Kilner J a. Layered perovskites as promising cathodes for intermediate temperature solid oxide fuel cells. J Mater Chem 2007;17:3175.
[17] Kim S, Jun A, Kwon O, Kim J, Yoo S. Nanostructured double perovskite cathode with low sintering temperature for intermediate temperature solid oxide fuel cells. ChemSusChem 2015;8. 3153–8.
[18] Haile SM. Fuel cell materials and components. Acta Mater 2003;51:5981–6000.
[19] Kim J, Choi S, Jun A, Jeong HY, Shin J, Kim G. Chemically stable perovskites as cathode materials for solid oxide fuel cells: La-doped $Ba_{0.5}Sr_{0.5}Co_{0.8}Fe_{0.2}O_{3-\delta}$. ChemSusChem 2014;7:1669–75.
[20] Zhao Y, Xia C, Jia L, Wang Z, Li H, Yu J, et al. Recent progress on solid oxide fuel cell: lowering temperature and utilizing non-hydrogen fuels. Int J Hydrogen Energy 2013;38:16498–517.
[21] Fabbri E, Pergolesi D, Licoccia S, Traversa E. Does the increase in Y-dopant concentration improve the proton conductivity of $BaZr_{1-x}Y_xO_{3-\delta}$fuel cell electrolytes? Solid State Ionics 2010;181:1043–51.
[22] Bohn HG, Schober T. Electrical conductivity of the high-temperature. J Am Ceram Soc 2000;72:768–72.
[23] Yamazaki Y, Hernandez-Sanchez R, Haile SM. High total proton conductivity in large-grained yttrium-doped barium zirconate. Chem Mater 2009;21:2755–62.
[24] Yamazaki Y, Blanc F, Okuyama Y, Buannic L, Lucio-Vega JC, Grey CP, et al. Proton trapping in yttrium-doped barium zirconate. Nat Mater 2013;12:647–51.
[25] Choi S, Kucharczyk CJ, Liang Y, Zhang X, Takeuchi I, Ji H-I, et al. Exceptional power density and stability at intermediate temperatures in protonic ceramic fuel cells. Nat Energy 2018;3:202–10.
[26] Rørvik PM, Haavik C, Griesche D, Schneller T, Lenrick F, Wallenberg LR. Chemical solution deposition of thin films for protonic ceramic fuel cells. Solid State Ionics 2014;262:852–5.
[27] Matsuzaki Y, Tachikawa Y, Somekawa T, Hatae T, Matsumoto H, Taniguchi S, et al. Effect of proton-conduction in electrolyte on electric efficiency of multi-stage solid oxide fuel cells. Sci Rep 2015;5:12640.
[28] Zhu H, Kee RJ. Modeling protonic-ceramic fuel cells with porous composite electrodes in a button-cell configuration. J Electrochem Soc 2017;164:F1400–11.
[29] Bi L, Boulfrad S, Traversa E. Steam electrolysis by solid oxide electrolysis cells (SOECs) with proton-conducting oxides. Chem Soc Rev 2014;43:8255–70.
[30] Tsekouras G, Neagu D, Irvine JTS. Step-change in high temperature steam electrolysis performance of perovskite oxide cathodes with exsolution of B-site dopants. Energy Environ Sci 2013;6:256.
[31] Wang S, Hao X, Zhan W. Research on a low temperature reversible solid oxide cell. Int J Hydrogen Energy 2017;42:29881–7.
[32] Jun A, Ju Y-W, Kim G. Solid oxide electrolysis: concluding remarks. Faraday Discuss 2015;00:1–10.
[33] Jun A, Kim J, Shin J, Kim G. Achieving high efficiency and eliminating degradation in solid oxide electrochemical cells using high oxygen-capacity perovskite. Angew Chem Int Ed 2016:1–5.
[34] Kim J, Jun A, Gwon O, Yoo S, Liu M, Shin J, et al. Hybrid-solid oxide electrolysis cell: a new strategy for efficient hydrogen production. Nano Energy 2018;44:121–6.
[35] Song SJ, Wachsman ED, Rhodes J, Dorris SE, Balachandran U. Hydrogen permeability of $SrCe_{1-x}MO_{3-\delta}$ (x = 0.05, M = Eu, Sm). Solid State Ionics 2004;167:99–105.
[36] Escolástico S, Ivanova M, Solís C, Roitsch S, Meulenberg WA, Serra JM. Improvement of transport properties and hydrogen permeation of chemically-stable proton-conducting oxides based on the system $BaZr_{1-x-y}Y_xM_yO_{3-\delta}$. RSC Adv 2012;2:4932–43.
[37] Bhide SV. Stability of $BaCeO_3$-based proton conductors in water-containing atmospheres. J Electrochem Soc 1999;146:2038.
[38] Zhang H, Wilhite BA. Electrical conduction and hydrogen permeation investigation on iron-doped barium zirconate membrane. J Membr Sci 2016;512:104–10.
[39] Meng X, Shang Y, Meng B, Yang N, Tan X, Sunarso J, et al. Bi-functional performances of $BaCe_{0.95}Tb_{0.05}O_{3-\delta}$-based hollow fiber membranes for power generation and hydrogen permeation. J Eur Ceram Soc 2016;36:4123–9.
[40] Liu M, Sun W, Li X, Feng S, Ding D, Chen D, et al. High-performance Ni-$BaZr_{0.1}Ce_{0.7}Y_{0.1}Yb_{0.1}O_{3-\delta}$(BZCYYb) membranes for hydrogen separation. Int J Hydrogen Energy 2013;38:14743–9.
[41] Zuo C, Lee TH, Dorris SE, Balachandran U, Liu M. Composite Ni-$Ba(Zr_{0.1}Ce_{0.7}Y_{0.2})O_3$ membrane for hydrogen separation. J Power Sources 2006;159:1291–5.
[42] Song SJ, Moon JH, Lee TH, Dorris SE, Balachandran U. Thickness dependence of hydrogen permeability for Ni-$BaCe_{0.8}Y_{0.2}O_{3-\delta}$. Solid State Ionics 2008;179:1854–7.
[43] Meng X, Song J, Yang N, Meng B, Tan X, Ma ZF, et al. Ni-$BaCe_{0.95}Tb_{0.05}O_{3-\delta}$ cermet membranes for hydrogen permeation. J Membr Sci 2012;401–402:300–5.
[44] Zhu Z, Sun W, Dong Y, Wang Z, Shi Z, Zhang Q, et al. Evaluation of hydrogen permeation properties of Ni-$Ba(Zr_{0.7}Pr_{0.1}Y_{0.2})O_{3-\delta}$ cermet membranes. Int J Hydrogen Energy 2014;39:11683–9.
[45] Liu W, Zhu Z, Sun W, Yan L, Liu W. Synthesis and hydrogen permeation of Ni-Ba$(Zr_{0.1}Ce_{0.7}Y_{0.2})O_{3-\delta}$ metal-ceramic asymmetric membranes. Int J Hydrogen Energy 2011;36:6337–42.
[46] Islam QA, Raja MW, Basu RN. Zr- and Tb-doped barium cerate-based cermet membrane for hydrogen separation application. J Am Ceram Soc 2017;100:1360–7.
[47] Escolástico S, Solís C, Kjølseth C, Serra JM. Outstanding hydrogen permeation through CO_2-stable dual-phase ceramic membranes. Energy Environ Sci 2014;7:3736–46.
[48] Rosensteel WA, Ricote S, Sullivan NP. Hydrogen permeation through dense $BaCe_{0.8}Y_{0.2}O_{3-\delta}$-$Ce_{0.8}Y_{0.2}O_{2-\delta}$ composite-ceramic hydrogen separation membranes. Int J Hydrogen Energy 2016;41:2598–606.
[49] Liu Z-W, Jun K-W, Roh H-S, Park S-E. Hydrogen production for fuel cells through methane reforming at low temperatures. J Power Sources 2002;111:283–7.
[50] Chaubey R, Sahu S, James OO, Maity S. A review on development of industrial processes and emerging techniques for production of hydrogen from renewable and sustainable sources. Renew Sustain Energy Rev 2013;23:443–62.
[51] Malerød-Fjeld H, Clark D, Yuste-Tirados I, Zanón R, Catalán-Martinez D, Beeaff D, et al. Thermo-electrochemical production of compressed hydrogen from methane with near-zero energy loss. Nat Energy 2017;2:923–31.
[52] Fu XZ, Luo JL, Sanger AR, Luo N, Chuang KT. Y-doped $BaCeO_{3-\delta}$ nanopowders as proton-conducting electrolyte materials for ethane fuel cells to co-generate ethylene and electricity. J Power Sources 2010;195:2659–63.
[53] Fu XZ, Luo JL, Sanger AR, Danilovic N, Chuang KT. An integral proton conducting SOFC for simultaneous production of ethylene and power from ethane. Chem Commun 2010;46:2052–4.
[54] Li M, Hua B, Luo J-L. Alternative fuel cell technologies for cogenerating electrical power and syngas from greenhouse gases. ACS Energy Lett 2017;2:1789–96.
[55] Morejudo SH, Zanón R, Escolástico S, Yuste-Tirados I, Malerød-Fjeld H, Vestre PK, et al. Direct conversion of methane to aromatics in a catalytic co-ionic membrane reactor. Science 2016;353:563–6.
[56] Ding D, Zhang Y, Wu W, Chen D, Liu M, He T. A novel low-thermal-budget approach for the co-production of ethylene and hydrogen via the electrochemical non-oxidative deprotonation of ethane. Energy Environ Sci 2018;11:1710–6.
[57] Sakbodin M, Wu Y, Oh SC, Wachsman ED, Liu D. Heterogeneous catalysis hydrogen-permeable tubular membrane reactor: promoting conversion and product selectivity for non-oxidative activation of methane over an Fe SiO_2 catalyst. Angewandte 2016;20742:16149–52.
[58] Marnellos G. Ammonia synthesis at atmospheric pressure. Science 1998;282:98–100.
[59] Panagos E, Voudouris I, Stoukides M. Modelling of equilibrium limited hydrogenation reactions carried out in H^+ conducting solid oxide membrane reactors. Chem Eng Sci 1996;51:3175–80.
[60] Ouzounidou M, Skodra A, Kokkofitis C, Stoukides M. Catalytic and electrocatalytic synthesis of NH_3 in a H^+ conducting cell by using an industrial Fe catalyst. Solid State Ionics 2007;178:153–9.
[61] Guo Y, Liu B, Yang Q, Chen C, Wang W, Ma G. Preparation via microemulsion method and proton conduction at intermediate-temperature of $BaCe_{1-x}Y_xO_{3-d}$. Electrochem Commun 2009;11:153–6.
[62] Skodra A, Stoukides M. Electrocatalytic synthesis of ammonia from steam and nitrogen at atmospheric pressure. Solid State Ionics 2009;180:1332–6.
[63] Wang X, Yin J, Xu J, Wang H, Ma G. Chemical stability, ionic conductivity of $BaCe_{0.9-x}Zr_xSm_{0.10}O_{3-d}$ and its application to ammonia synthesis at atmospheric pressure. Chin J Chem 2011;29:1114–8.
[64] Zhang M, Xu J, Ma G. Proton conduction in $Ba_xCe_{0.8}Y_{0.2}O_{3-d}$ + 0.04ZnO at intermediate temperatures and its application in ammonia synthesis at atmospheric pressure. J Mater Sci 2011;46:4690–4.
[65] Klinsrisuk S, Irvine JTS. Electrocatalytic ammonia synthesis via a proton conducting oxide cell with $BaCe_{0.5}Zr_{0.3}Y_{0.16}Zn_{0.04}O_{3-d}$ electrolyte membrane. Catal Today 2017;286:41–50.
[66] Vasileiou E, Kyriakou V, Garagounis I, Vourros A, Manerbino A, Coors WG, et al.

Electrochemical enhancement of ammonia synthesis in a $BaZr_{0.7}Ce_{0.2}Y_{0.1}O_{2.9}$ solid electrolyte cell. Solid State Ionics 2016;288:357–62.
[67] Chen CH, Chang SJ, Chang SP, Li MJ, Chen IC, Hsueh TJ, et al. Novel fabrication of UV photodetector based on ZnO nanowire/p-GaN heterojunction. Chem Phys Lett 2009;476:69–72.
[68] Yin J, Wang X, Xu J, Wang H, Zhang F, Ma G. Ionic conduction in $BaCe_{0.85}$ -$XZr_xEr_{0.15}O_{3-\alpha}$ and its application to ammonia synthesis at atmospheric pressure. Solid State Ionics 2011;185:6–10.
[69] Chen C, Ma G. Proton conduction in $BaCe_{1-x}Gd_xO_{3-d}$ at intermediate temperature and its application to synthesis of ammonia at atmospheric pressure. J Alloy Comp 2009;485:69–72.
[70] Duan C, Tong J, Shang M, Nikodemski S, Sanders M, Ricote S, et al. Readily processed protonic ceramic fuel cells with high performance at low temperatures. Science 2015;349:1321–6.
[71] Peng R, Wu T, Liu W, Liu X, Meng G. Cathode processes and materials for solid oxide fuel cells with proton conductors as electrolytes. J Mater Chem 2010;20:6218.
[72] Uchida H, Tanaka S, Iwahara H. Polarization at Pt electrodes of a fuel cell with a high temperature-type proton conductive solid electrolyte. J Appl Electrochem 1985;15:93–7.
[73] He F, Wu T, Peng R, Xia C. Cathode reaction models and performance analysis of $Sm_{0.5}Sr_{0.5}CoO_{3-\delta}$–$BaCe_{0.8}Sm_{0.2}O_{3-\delta}$ composite cathode for solid oxide fuel cells with proton conducting electrolyte. J Power Sources 2009;194:263–8.
[74] Poetzsch D, Merkle R, Maier J. Oxygen reduction at dense thin-film microelectrodes on a proton-conducting electrolyte: I. Considerations on reaction mechanism and electronic leakage effects. J Electrochem Soc 2015;162:F939–50.
[75] Steele BCH, Heinzel A. Materials for fuel-cell technologies. Nature 2001;414:345–52.
[76] Wu T, Peng R, Xia C. $Sm_{0.5}Sr_{0.5}CoO_{3-d}$-$BaCe_{0.8}Sm_{0.2}O_{3-d}$ composite cathodes for proton-conducting solid oxide fuel cells. Solid State Ionics 2008;179:1505–8.
[77] Pergolesi D, Fabbri E, Traversa E. Chemically stable anode-supported solid oxide fuel cells based on Y-doped barium zirconate thin films having improved performance. Electrochem Commun 2010;12:977–80.
[78] Fabbri E, Bi L, Rupp JLM, Pergolesi D, Traversa E. Electrode tailoring improves the intermediate temperature performance of solid oxide fuel cells based on a Y and Pr co-doped barium zirconate proton conducting electrolyte. RSC Adv 2011;1:1183.
[79] Sun W, Liu M, Liu W. Chemically stable yttrium and tin Co-doped barium zirconate electrolyte for next generation high performance proton-conducting solid oxide fuel cells. Adv Energy Mater 2013;3:1041–50.
[80] Kim J, Sengodan S, Kwon G, Ding D, Shin J. Triple-conducting layered perovskites as cathode materials for proton-conducting solid oxide fuel cells. 2014. 2811–5.
[81] Bae K, Jang DY, Choi HJ, Kim D, Hong J, Kim B-K, et al. Demonstrating the potential of yttrium-doped barium zirconate electrolyte for high-performance fuel cells. Nat Commun 2017;8:14553.
[82] Duan C, Tong J, Shang M, Nikodemski S, Sanders M, Ricote S, et al. Readily processed protonic ceramic fuel cells with high performance at low temperatures. Science 2015;349.
[83] Xiao J, Sun W, Zhu Z, Tao Z, Liu W. Fabrication and characterization of anode-supported dense $BaZr_{0.8}Y_{0.2}O_{3-\delta}$ electrolyte membranes by a dip-coating process. Mater Lett 2012;73:198–201.
[84] Tao Z, Bi L, Yan L, Sun W, Zhu Z, Peng R, et al. A novel single phase cathode material for a proton-conducting SOFC. Electrochem Commun 2009;11:688–90.
[85] Lee S, Park I, Lee H, Shin D. Continuously gradient anode functional layer for BCZY based proton-conducting fuel cells. Int J Hydrogen Energy 2014;39:14342–8.
[86] Sun W, Yan L, Shi Z, Zhu Z, Liu W. Fabrication and performance of a proton-conducting solid oxide fuel cell based on a thin $BaZr_{0.8}Y_{0.2}O_{3-\delta}$ electrolyte membrane. J Power Sources 2010;195:4727–30.
[87] Fabbri E, Bi L, Tanaka H, Pergolesi D, Traversa E. Chemically stable Pr and Y Co-doped barium zirconate electrolytes with high proton conductivity for intermediate-temperature solid oxide fuel cells. Adv Funct Mater 2011;21:158–66.
[88] An H, Lee HW, Kim BK, Son JW, Yoon KJ, Kim H, et al. A 5 × 5 cm^2 protonic ceramic fuel cell with a power density of 1.3 W cm^{-2} at 600 °C. Nat Energy 2018;3:1–6.
[89] Bae K, Kim DH, Choi HJ, Son JW, Shim JH. High-performance protonic ceramic fuel cells with 1 μm thick Y:Ba(Ce, Zr)O_3 electrolytes. Adv Energy Mater 2018;8:1–4.
[90] Grimaud A, Mauvy F, Bassat JM, Fourcade S, Rocheron L, Marrony M, et al. Hydration properties and rate determining steps of the oxygen reduction reaction of perovskite-related oxides as H^+-SOFC cathodes. J Electrochem Soc 2012;159:B683.
[91] Lin B, Zhang S, Zhang L, Bi L, Ding H, Liu X, et al. Protonic ceramic membrane fuel cells with layered $GdBaCo_2O_{5+x}$ cathode prepared by gel-casting and suspension spray. J Power Sources 2008;177:330–3.
[92] Lin B, Dong Y, Yan R, Zhang S, Hu M, Zhou Y, et al. In situ screen-printed BaZr0.1Ce0.7Y0.2O3 − δ electrolyte-based protonic ceramic membrane fuel cells with layered $SmBaCo_2O_{5+x}$ cathode. J Power Sources 2009;186:446–9.
[93] Jin M, Zhang X, Qiu Y, Sheng J. Layered $PrBaCo_2O_{5+\delta}$ perovskite as a cathode for proton-conducting solid oxide fuel cells. J Alloy Comp 2010;494:359–61.
[94] Ding H, Xue X. Proton conducting solid oxide fuel cells with layered $PrBa_{0.5}Sr_{0.5}Co_2O_{5+\delta}$ perovskite cathode. Int J Hydrogen Energy 2010;35:2486–90.
[95] Ding H, Xue X, Liu X, Meng G. A novel layered perovskite cathode for proton conducting solid oxide fuel cells. J Power Sources 2010;195:775–8.
[96] Nian Q, Zhao L, He B, Lin B, Peng R, Meng G, et al. Layered $SmBaCuCoO_{5+\delta}$ and $SmBaCuFeO_{5+\delta}$ perovskite oxides as cathode materials for proton-conducting SOFCs. J Alloy Comp 2010;492:291–4.
[97] Ding H, Xue X. Novel layered perovskite $GdBaCoFeO_{5+\delta}$ as a potential cathode for proton-conducting solid oxide fuel cells. Int J Hydrogen Energy 2010;35:4311–5.
[98] Lin Y, Ran R, Zheng Y, Shao Z, Jin W, Xu N, et al. Evaluation of $Ba_{0.5}Sr_{0.5}Co_{0.8}Fe_{0.2}O_{3-\delta}$ as a potential cathode for an anode-supported proton-conducting solid-oxide fuel cell. J Power Sources 2008;180:15–22.
[99] Bi L, Shafi SP, Husni E, Traversa E. Tailoring the cathode – electrolyte interface with nanoparticles for boosting the solid oxide fuel cell performance of chemically stable proton-conducting electrolytes. 2018. p. 1–9. 1801231.
[100] Yamaura H, Ikuta T, Yahiro H, Okada G. Cathodic polarization of strontium-doped lanthanum ferrite in proton-conducting solid oxide fuel cell. Solid State Ionics 2005;176:269–74.
[101] Tao Z, Bi L, Zhu Z, Liu W. Novel cobalt-free cathode materials $BaCe_xFe_{1-x}O_{3-\delta}$ for proton-conducting solid oxide fuel cells. J Power Sources 2009;194:801–4.
[102] Mao X, Yu T, Ma G. Performance of cobalt-free double-perovskite $NdBaFe_{2-x}Mn_xO_{5+\delta}$ cathode materials for proton-conducting IT-SOFC. J Alloy Comp 2015;637:286–90.
[103] Mukundan R, Davies PK, Worrell WL. Electrochemical characterization of mixed conducting $Ba(Ce_{0.8-y}Pr_yGd_{0.2})O_{2.9}$ cathodes. J Electrochem Soc 2001;148:A82.
[104] Magrasó A, Haugsrud R, Segarra M, Norby T. Defects and transport in Gd-doped $BaPrO_3$. J Electroceram 2009;23:80–8.
[105] Fabbri E, Oh T, Licoccia S, Traversa E, Wachsman ED. Mixed protonic/electronic conductor cathodes for intermediate temperature SOFCs based on proton conducting electrolytes. J Electrochem Soc 2009;156:B38.
[106] Zohourian R, Merkle R, Maier J. Proton uptake into the protonic cathode material $BaCo_{0.4}Fe_{0.4}Zr_{0.2}O_{3-\delta}$ and comparison to protonic electrolyte materials. Solid State Ionics 2016:6–11.
[107] Poetzsch D, Merkle R, Maier J. Stoichiometry variation in materials with three mobile carriers-Thermodynamics and transport kinetics exemplifi ed for protons, oxygen vacancies, and holes. Adv Funct Mater 2015;25:1542–57.
[108] Shang M, Tong J, O'Hayre R. A promising cathode for intermediate temperature protonic ceramic fuel cells: $BaCo_{0.4}Fe_{0.4}Zr_{0.2}O_{3-\delta}$. RSC Adv 2013;3:15769.
[109] Fabbri E, Licoccia S, Traversa E, Wachsman ED. Composite cathodes for proton conducting electrolytes. Fuel Cells 2009;9:128–38.
[110] Bi L, Fabbri E, Sun Z, Traversa E. A novel ionic diffusion strategy to fabricate high-performance anode-supported solid oxide fuel cells (SOFCs) with proton-conducting Y-doped $BaZrO_3$ films. Energy Environ Sci 2011;4:409.
[111] Zunic M, Chevallier L, Deganello F, D'Epifanio A, Licoccia S, Di Bartolomeo E, et al. Electrophoretic deposition of dense $BaCe_{0.9}Y_{0.1}O_{3-x}$ electrolyte thick-films on Ni-based anodes for intermediate temperature solid oxide fuel cells. J Power Sources 2009;190:417–22.
[112] Zunic M, Chevallier L, Di Bartolomeo E, D'Epifanio A, Licoccia S, Traversa E. Anode supported protonic solid oxide fuel cells fabricated using electrophoretic deposition. Fuel Cells 2011;11:165–71.
[113] Geneste G. Proton transfer in barium zirconate: lattice reorganization, Landau-Zener curve-crossing approach. Solid State Ionics 2018;323:172–202.
[114] Stokes SJ, Islam MS. Defect chemistry and proton-dopant association in $BaZrO_3$ and $BaPrO_3$. J Mater Chem 2010;20:6258.
[115] Kreuer KD. Proton-conducting oxides. Annu Rev Mater Res 2003;33:333–59.
[116] Kreuer KD, Adams S, Münch W, Fuchs A, Klock U, Maier J. Proton conducting alkaline earth zirconates and titanates for high drain electrochemical applications. Solid State Ionics 2001;145:295–306.
[117] Gopalan S, Virkar AV. Thermodynamic stabilities of $SrCeO_3$ and $BaCeO_3$ using a molten salt method and galvanic cells. J Electrochem Soc 1993;140:1060.
[118] Magrasó A, Fontaine ML, Larring Y, Bredesen R, Syvertsen GE, Lein HL, et al. Development of proton conducting SOFCs based on $LaNbO_4$electrolyte - status in Norway. Fuel Cells 2011;11:17–25.
[119] Matsumoto H, Kawasaki Y, Ito N, Enoki M, Ishihara T. Relation between electrical conductivity and chemical stability of $BaCeO_3$-based proton conductors with different trivalent dopants. Electrochem Solid State Lett 2007;10:B77.
[120] Sun Z, Fabbri E, Bi L, Traversa E. Lowering grain boundary resistance of $BaZr_{0.8}Y_{0.2}O_{3-\delta}$ with $LiNO_3$ sintering-aid improves proton conductivity for fuel cell operation. Phys Chem Chem Phys 2011;13:7692–700.
[121] Tong J, Clark D, Hoban M, Hayre RO. Cost-effective solid-state reactive sintering method for high conductivity proton conducting yttrium-doped barium zirconium ceramics. Solid State Ionics 2010;181:496–503.
[122] Bi L, Da'as EH, Shafi SP. Proton-conducting solid oxide fuel cell (SOFC) with Y-doped $BaZrO_3$ electrolyte. Electrochem Commun 2017;80:20–3.
[123] Pergolesi D, Fabbri E, D'Epifanio A, Di Bartolomeo E, Tebano A, Sanna S, et al. High proton conduction in grain-boundary-free yttrium-doped barium zirconate films grown by pulsed laser deposition. Nat Mater 2010;9:846–52.
[124] Shim JH, Gür TM, Prinz FB. Proton conduction in thin film yttrium-doped barium zirconate. Appl Phys Lett 2008;92:253115.
[125] Kreuer K. On the development of proton conducting materials for technological applications. Solid State Ionics 1997;97:1–15.
[126] Zuo C, Wang JH, Liu M, Technologies B. Development of novel electrolyte materials for a new generation of low-temperature SOFCs final report for year 2. 2007.
[127] Xu X, Tao S, Irvine JTS. Proton conductivity of potassium doped barium zirconates. J Solid State Chem 2010;183:93–8.
[128] Ryu KH, Haile SM. Chemical stability and proton conductivity of doped $BaCeO_3$–$BaZrO_3$ solid solutions. Solid State Ionics 1999;125:355–67.
[129] Lü J, Wang L, Fan L, Li Y, Dai L, Guo H. Chemical stability of doped $BaCeO_3$-$BaZrO_3$ solid solutions in different atmospheres. J Rare Earths 2008;26:505–10.
[130] Taniguchi N, Nishimura C, Kato J. Endurance against moisture for protonic conductors of perovskite-type ceramics and preparation of practical conductors. Solid State Ionics 2001;145:349–55.
[131] Yang L, Wang S, Blinn K, Liu M, Liu Z, Cheng Z, et al. Enhanced sulfur and coking tolerance of a mixed ion conductor for SOFCs: $BaZr_{0.1}Ce_{0.7}Y_{0.2-x}Yb_xO_{3-d}$. Science

2009;326:126–9.
[132] Haugsrud R, Norby T. Proton conduction in rare-earth ortho-niobates and ortho-tantalates. Nat Mater 2006;5:193–6.
[133] Haugsrud R, Norby T. High-temperature proton conductivity in acceptor-doped LaNbO4. Solid State Ionics 2006;177:1129–35.
[134] Atkinson A, Barnett S, Gorte RJ, Irvine JTS, McEvoy a J, Mogensen M, et al. Advanced anodes for high-temperature fuel cells. Nat Mater 2004;3:17–27.
[135] Coors WG, Manerbino A. Characterization of composite cermet with 68 wt.% NiO and $BaCe_{0.2}Zr_{0.6}Y_{0.2}O_{3-\delta}$. J Membr Sci 2011;376:50–5.
[136] Yang L, Wang S, Blinn K, Liu M, Liu Z, Cheng Z, et al. Enhanced sulfur and coking tolerance of a mixed ion conductor for SOFCs: $BaZr_{0.1}Ce_{0.7}Y_{0.2-x}Yb_xO_{3-d}$. Science 2009;326:126–9.
[137] Bonanos N. Transport properties and conduction mechanism in high-temperature protonic conductors. Solid State Ionics 1992;53–56:967–74.
[138] Zhao F, Virkar AV. Dependence of polarization in anode-supported solid oxide fuel cells on various cell parameters. J Power Sources 2005;141:79–95.
[139] Rainwater BH, Liu M, Liu M. A more efficient anode microstructure for SOFCs based on proton conductors. Int J Hydrogen Energy 2012;37:18342–8.
[140] Information S. Layered oxygen-deficient double perovskite as an efficient and stable anode for direct hydrocarbon solid oxide fuel cells. Nat Mater 2014:1–27.
[141] Liu M, Lynch ME, Blinn K, Alamgir FM, Choi Y. Rational SOFC material design: new advances and tools. Mater Today 2011;14:534–46.
[142] Toebes ML, Bitter JH, van Dillen AJ, de Jong KP. Impact of the structure and reactivity of nickel particles on the catalytic growth of carbon nanofibers. Catal Today 2002;76:33–42.
[143] Cheng Z, Liu M. Characterization of sulfur poisoning of Ni–YSZ anodes for solid oxide fuel cells using in situ Raman microspectroscopy. Solid State Ionics 2007;178:925–35.
[144] Zha S, Cheng Z, Liu M. Sulfur poisoning and regeneration of Ni-based anodes in solid oxide fuel cells. J Electrochem Soc 2007;154:B201.
[145] Cheng Z, Wang J-H, Choi Y, Yang L, Lin MC, Liu M. From Ni-YSZ to sulfur-tolerant anode materials for SOFCs: electrochemical behavior, in situ characterization, modeling, and future perspectives. Energy Environ Sci 2011;4:4380.
[146] Kwon O, Sengodan S, Kim K, Kim G, Jeong HY, Shin J, et al. Exsolution trends and co-segregation aspects of self-grown catalyst nanoparticles in perovskites. Nat Commun 2017;8:15967.
[147] Ge XM, Chan SH, Liu QL, Sun Q. Solid oxide fuel cell anode materials for direct hydrocarbon utilization. Adv Energy Mater 2012;2:1156–81.
[148] Wang W, Su C, Wu Y, Ran R, Shao Z. Progress in solid oxide fuel cells with nickel-based anodes operating on methane and related fuels. Chem Rev 2013;113:8104–51.
[149] Huang Y-H, Dass RI, Xing Z-L, Goodenough JB. Double perovskites as anode. Science 2006;2:254–8.
[150] Corre G, Kim G, Cassidy M, Vohs JM, Gorte RJ, Irvine JTS. Activation and ripening of impregnated manganese containing perovskite sofc electrodes under redox cycling. Chem Mater 2009;21:1077–84.
[151] Sengodan S, Yoon JS, Yoon MY, Hwang HJ, Shin J, Kim G. Electrochemical performance of YST infiltrated and Fe doped YST infiltrated YSZ anodes for IT-SOFC. ECS Electrochem Lett 2013;2:F45–9.
[152] Sengodan S, Yeo HJ, Shin JY, Kim G. Assessment of perovskite-type $La_{0.8}Sr_{0.2}Sc_xMn_{1-x}O_{3-\delta}$ oxides as anodes for intermediate-temperature solid oxide fuel cells using hydrocarbon fuels. J Power Sources 2011;196:3083–8.
[153] Yang L, Wang S, Blinn K, Liu M, Liu Z, Cheng Z, et al. Enhanced sulfur and coking tolerance of a mixed ion conductor for SOFCs: $BaZr_{0.4}Ce_{0.4}Y_{0.1}Yb_{0.1}O_{3-\delta}$. Science 2009;326:126–9.
[154] Blinn KS, Abernathy H, Li X, Liu M, Bottomley LA, Liu M. Raman spectroscopic monitoring of carbon deposition on hydrocarbon-fed solid oxide fuel cell anodes. Energy Environ Sci 2012;5:7913.
[155] Blinn KS, Liu M. $BaZr_{0.9}Yb_{0.1}O_{3-\delta}$-modified bi-electrode supported solid oxide fuel cells with enhanced coking and sulfur tolerance. J Power Sources 2013;243:24–8.
[156] Liu M, Choi Y, Yang L, Blinn K, Qin W, Liu P, et al. Direct octane fuel cells: a promising power for transportation. Nano Energy 2012;1:448–55.
[157] Kwon O, Sengodan S, Lim C, Jeong HY, Shin J, Ju Y-W, et al. In situ surface modification of Ni-YSZ with $BaZrO_3$ for enhancing the sulfur tolerance of Ni-YSZ anode. J Electrochem Soc 2016;163:F1055–8.
[158] Sengodan S, Liu M, Lim T-H, Shin J, Kim G. Enhancing sulfur tolerance of a Ni-YSZ anode through $BaZr_{0.1}Ce_{0.7}Y_{0.1}Yb_{0.1}O_{3-d}$ infiltration. J Electrochem Soc 2014;161:F668–73.
[159] Duan C, Kee RJ, Zhu H, Karakaya C, Chen Y, Ricote S, et al. Highly durable, coking and sulfur tolerant, fuel-flexible protonic ceramic fuel cells. Nature 2018;557:217–22.